MATERIALS AND METHODS

(−)-^{3}H-Cytisine (1.48 TBq mmol) was purchased from NEN Life Science Products, Inc. Nonradioactive 5MA was synthesized according to the method of Karimi and Langstrom (*29*), and its structure was confirmed by proton nuclear magnetic resonance, mass spectrometry, and elemental analyses. All other chemicals used were of reagent grade. Male ddY mice and Wistar rats were supplied by Japan SLC Co. Ltd. and male rhesus monkeys (*Macaca mulatta*) were obtained from Clea Japan, Inc. The animal studies were conducted according to guidelines stipulated by the Kyoto University Animal Care and Use Committee.

Radiosynthesis of ^{11}C-5MA

^{11}C was produced via a ^{14}N(p, α)^{11}C reaction with 11.3-MeV protons on a target of nitrogen gas by an ultracompact cyclotron (CYPRIS model 325; Sumitomo Heavy Industry Ltd.). The $^{11}CO_2$ produced was transported to an automated synthesis system of ^{11}C-methyl iodide (CUPID C-100; Sumitomo Heavy Industry Ltd.). The synthesis of ^{11}C-5MA is outlined in Figure 1. A precursor, 5-(tri-*n*-butylstannyl)-3-((*S*)-1-(*tert*-butoxycarbonyl)-2-azetidinylmethoxy)pyridine, was prepared according to methods described in the literature (*21,25,27*). The precursor (1 mg) was dissolved in 0.5 mL of freshly distilled *N,N*-dimethylformamide and added into the reaction vessel containing tris(dibenzylideneacetone)dipalladium (4.6 mg), tri-*o*-tolylphosphine (6.1 mg), CuCl (2.0 mg), and K_2CO_3 (2.8 mg) under argon gas. The ^{11}C-methyl iodide synthesized was transferred to the reaction vessel via a nitrogen stream. After heating at 80°C for 3 min, the vessel was cooled with chilled air. Cleavage of the *tert*-butoxycarbonyl protection was achieved by adding 1.0 mL of trifluoroacetic acid and heating at 100°C for 5 min. After neutralization with the 6N NaOH solution, the reaction solution was diluted with 10 mL of water and loaded on an OASIS column (Waters). After the column was washed with 2 mL of aqueous 5% methanol solution, radioactivity was eluted with 0.5 mL of methanol. The eluted methanol solution was then applied to a preparative high-performance liquid chromatography column (COSMOSIL 5C18-AR-300, 10 × 250 mm; Nakalai), and ^{11}C-5MA was eluted with 0.6% triethylamine in acetonitrile and 0.01 mol L ammonium acetate (3:1) at a flow rate 3.5 mL min (retention time = 12 min for ^{11}C-5MA). After collection of the radioactivity of ^{11}C-5MA, the organic solvent was removed in vacuo. The residue was diluted with saline and filtered through a sterile 0.2-μm membrane filter into a sterile vial.

In Vitro nAChR-Binding Studies

The affinity of 5MA for nAChRs was measured on the basis of the displacement of (−)-^{3}H-cytisine from a preparation of rat cerebral cortical synaptosomal membranes, according to the method of Pabreza et al. (*30*) with a slight modification. In brief, the cerebral cortex of male Wistar rats (230–250 g) was homogenized in 50 mmol L Tris-HCl buffer (pH 7.4) containing 120 mmol L NaCl, 5 mmol L KCl, 1 mmol L $MgCl_2$, and 2.5 mmol L $CaCl_2$ with a Polytron (Brinkmann). The homogenate was then centrifuged at 45,000*g* for 10 min at 4°C, and the pellet was resuspended in fresh buffer to yield a synaptosomal membrane suspension with a protein concentration of 1 mg mL.

Binding assays were performed by incubation of 0.1 mL of the cortical synaptosomal membrane suspension (1 mg protein) at 2°C with (−)-^{3}H-cytisine (5 nmol L) and various concentrations of competing drugs in 0.15 mL of 50 mmol L Tris-HCl buffer (pH 7.4) containing 120 mmol L NaCl, 5 mmol L KCl, 1 mmol L $MgCl_2$, and 2.5 mmol L $CaCl_2$. When acetylcholine was used in competition studies, 200 μmol L diisopropyl fluorophosphate, a cholinesterase inhibitor, was added to the tissue homogenate approximately 30 min before initiation of the assay. Incubation was performed for 75 min at 2°C, after which the samples were rapidly filtered through polylysine-soaked Whatman GF/C filters, and the filters were washed rapidly 3 times with 4 mL of ice-cold assay buffer. Each filter was then placed into a 20-mL scintillation vial containing 10 mL ACS II (Amersham) and the radioactivity bound to the filter was measured with a liquid scintillation counter. The 50% inhibitory concentration (IC_{50}) values were determined from displacement curves of the percentage inhibition of (−)-^{3}H-cytisine binding versus the inhibitor concentration by means of the LIGAND curve-fitting computer program (Elsevier-Biosoft). For calculation of the inhibition constant (K_i), the value of 0.96 nmol L obtained by Pabreza et al. was used as the dissociation constant (K_d) for (−)-cytisine (*30*).

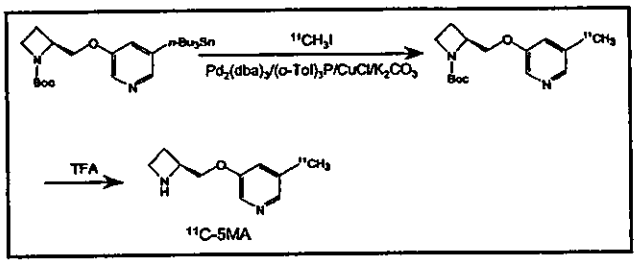

FIGURE 1. Radiosynthesis of ^{11}C-5MA. TFA = trifluoroacetic acid.

Determination of Brain Uptake Index (BUI)

To assess the permeability of the blood–brain barrier, a BUI study was performed in rats using the double-isotope, intracarotid, single-injection technique of Oldendorf (*31*). Briefly, a mixture of 200 μL of saline containing ^{11}C-5MA (3,700 kBq) and ^{14}C-butanol (37 kBq) was injected into the right common carotid artery of male Wistar rats (250 g), and the rats were killed by decapitation 15 s after the injection. Part of the cortex was removed from each rat and the ^{11}C radioactivity was measured in a NaI well scintillation counter. After all ^{11}C had decayed, the samples were treated with NCS tissue solubilizer (Amersham) and the ^{14}C radioactivity was measured in a liquid scintillation counter. Finally, the BUI was calculated according to the following formula:

$$BUI = ([^{11}C \text{ in brain (kBq)}\ ^{14}C \text{ in brain (kBq)}] / [\text{Injected } ^{11}C \text{ (kBq) Injected } ^{14}C \text{ (kBq)}]) \times 100.$$

Biodistribution Studies in Mice

Male ddY mice weighing about 30 g were injected via the tail vein with 3.7 MBq ^{11}C-5MA in 0.1 mL of saline solution. At the designated times after injection, the mice were killed by decapitation and their organs were removed. Then the tissues were weighed and the radioactivity was measured in a NaI well scintillation counter.

The relative binding affinity of ^{11}C-5MA for nicotinic acetylcholine receptors was determined with various drugs, which were injected into mice given 3.7 MBq ^{11}C-5MA. (−)-Cytisine (1 mg/kg), (−)-nicotine (60 μg/kg), dexetimide (10 mg/kg), and 5MA (0.1 mg/kg) were injected intravenously 5 min before the radioligand, whereas scopolamine (10 mg/kg) and mecamylamine

(5 mg/kg) were injected subcutaneously 30 min before the radioligand. The mice were killed 30 min after administration of the radioligand; then the brain regions were dissected and the radioactivity was measured in a NaI well scintillation counter.

Metabolic Studies

Male ddY mice weighing about 30 g were injected intravenously with 111 MBq ^{11}C-5MA and then decapitated 30 min after injection. The brains were removed immediately and homogenized in 1 mL of methanol. After centrifugation at 1,750*g* for 5 min at 4°C, the precipitate was washed with 1 mL of methanol and the wash was combined with the supernatant. The combined methanol extracts were evaporated under a stream of nitrogen to a small volume and analyzed by thin-layer chromatography (methanol: 10% ammonium acetate aqueous solution, 1:1; R_f = 0.43–0.50 for ^{11}C-5MA).

PET Study of ^{11}C-5MA in Rhesus Monkey

PET studies were performed on a male rhesus monkey (*M. mulatta*), 3.9 kg in body weight, with a multislice PET scanner for animals (SHR-7700; Hamamatsu Photonics K.K.) (*32,33*). This scanner provided 31 slices of tomographic images at 3.6-mm intervals per frame. Transaxial resolution of the system was 2.6-mm full width at half maximum at the center of the field of view. PET images were reconstructed by the filtered-backprojection method with a Hanning 4.5-mm filter.

After an overnight fast, a monkey was seated in the monkey chair and fixed with stereotactic coordinates aligned parallel to the orbitomeatal line. A cannula was implanted into the posterior tibial vein for administration of a radiolabeled compound. The PET scans were performed under dim light. Eight hundred megabecquerels of ^{11}C-5MA were injected through the posterior tibial vein cannula. Each PET scan was performed for 121 min with 6 time frames at 10-s intervals, 6 time frames at 30 s, and 12 time frames at 1 min, followed by 35 time frames at 3 min. Regions of interest (ROIs) were identified in 7 cortical regions (frontal, temporal and occipital cortices, striatum, cingulate gyrus, thalamus, and cerebellum) according to MR images, and time–activity curves in ROIs were obtained. Activities in ROIs were calibrated using the cross-calibration factor calculated in the phantom study with a 10-cm-diameter hollow phantom.

In the displacement studies, 5 mg/kg of (−)-cytisine were injected intravenously 90 min before or 50 min after administration of ^{11}C-5MA (800 MBq). The scanning was performed with the same procedure as in the control study.

Statistical Analysis

Data are presented as mean ± SD. Comparisons between groups were performed with the Dunnett multiple comparisons test. $P < 0.05$ was considered statistically significant.

RESULTS

Radiosynthesis of ^{11}C-5MA

^{11}C-5MA was synthesized by the incorporation of ^{11}C-methyl iodide into the stannyl compound using a Pd-catalyzed coupling reaction, followed by deprotection of the *N*-butoxycarbonyl group with acidic condition, referring to the report of Karimi and Langstrom (*29*) and the report of Suzuki et al. (*34*); we used the tributylstannyl compound instead of the trimethylstannyl compound as a precursor and *N,N*-dimethylformamide instead of dimethyl sulfoxide as a solvent (Fig. 1). The tributylstannyl compound has the advantage that it can also be used as a precursor in the synthesis of ^{123}I-iodinated A-85380 (5IA), a SPECT radiopharmaceutical for nAChRs (*21,25,27*). The overall synthesis time including the final formulation in saline was 60 min from the end of radionuclide production, and the overall decay-corrected radiochemical yield of ^{11}C-5MA was 30% calculated from the amount of ^{11}C-methyl iodide. The radiochemical purity of the product was >99%, with a specific radioactivity of >36 GBq/μmol, estimated from ultraviolet absorbance at 274 nm.

In Vitro Binding

Using the reference compounds, A-85380, (−)-cytisine, (−)-nicotine, acetylcholine, mecamylamine, and α-bungarotoxin, the affinity of 5MA for brain nAChRs was measured by examining competition with (−)-^{3}H-cytisine for binding sites in rat cortical membranes. Figure 2 illustrates competitive binding curves representative of these compounds, and the K_i values determined from IC_{50} are summarized in Table 1. 5MA showed approximately 1.5-fold higher affinity than A-85380, 3-fold higher affinity than (−)-cytisine, and 10-fold higher affinity than (−)-nicotine. Since A85380, (−)-cytisine, and (−)-nicotine are compounds with high affinity for central nAChRs (*12,18,30*), these results indicate that 5MA showed high binding affinity for nAChRs.

Determination of BUI

The BUI of ^{11}C-5MA was investigated in rats. ^{11}C-5MA showed a moderate BUI (mean ± SD = 9.4 ± 3.1 with respect to the ^{14}C-butanol reference).

Biodistribution Studies in Mice

The results of the radioactivity distribution studies in mice after intravenous administration of ^{11}C-5MA are summarized in Table 2. ^{11}C-5MA gradually entered the brain

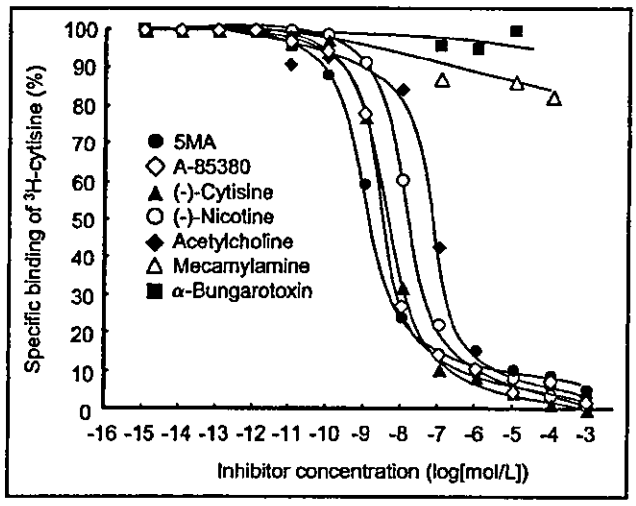

FIGURE 2. Inhibition of (−)-^{3}H-cytisine binding to rat cortical membranes by various drugs.

TABLE 1
K_i Values for Inhibiting (−)-^{3}H-Cytisine Binding to Rat Brain Synaptosomal Membranes

Compound	K_i (nmol/L)
5MA	0.27 ± 0.16*
A-85380	0.38 ± 0.01*
(−)-Cytisine	0.92 ± 0.42*
(−)-Nicotine	2.71 ± 0.73*
Acetylcholine	13.40 ± 2.61*
Mecamylamine	>1,000,000†
α-Bungarotoxin	>1,000,000†

*Mean ± SD of 3 independent experiments.
†Not inhibited at the highest concentration tested (10^{-4} mol/L).

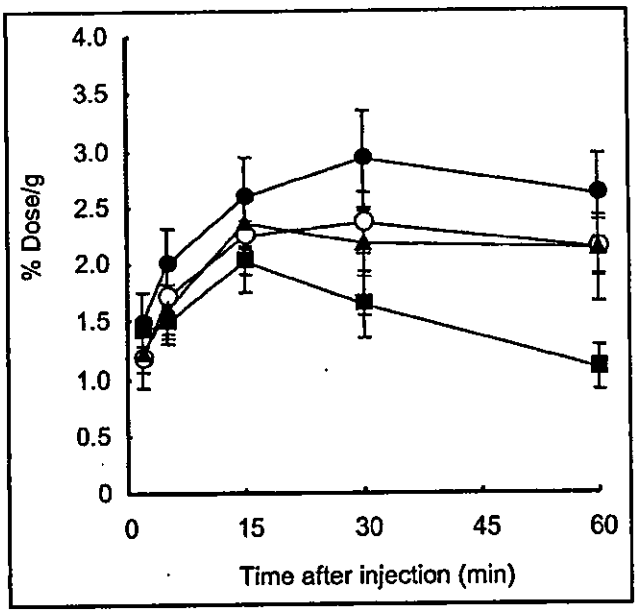

FIGURE 3. Regional brain uptake of ^{11}C-5MA in mice. ●, Thalamus; ○, cortex; ▲, striatum; ■, cerebellum. Data are presented as mean ± SD.

and a high uptake of radioactivity was observed over 15–30 min, after which there was a decline with time. The radioactivity in blood was cleared rapidly. The brain-to-blood ratio of radioactivity increased with time, and the highest ratio was 4.3 at 60 min after injection. A high initial uptake was also observed in the kidneys, pancreas, liver, and lungs, but the radioactivity in these organs cleared rapidly. No abnormality was observed in behavior after injection of ^{11}C-5MA.

The temporal distribution of the radioactivity in various regions of the mouse brain is shown in Figure 3. Differences in the regional distribution of radioactivity were observed—that is, the thalamus showed the highest uptake, followed by the cortex, striatum, and cerebellum in that order. The thalamus-to-cerebellum ratio gradually increased with time, and the highest value was 2.5 at 60 min. The regional distribution of ^{11}C-5MA at 30 min parallels the distribution of nAChRs determined by the in vitro binding assay (*35*) ($r = 0.97$) (Fig. 4). Furthermore, the effects of various drugs on the levels of ^{11}C-5MA in various regions were studied. As shown in Figure 5, the administration of (−)-nicotine and (−)-cytisine, compounds with high affinity for central nAChRs (*13,18,30,36*), reduced the uptake of radioactivity at higher magnitude in the region of higher uptake in the untreated brain and resulted in almost the same level throughout the brain. Similar results were observed in the treatment with nonradioactive 5MA. However, the administration of dexetimide and scopolamine, drugs with high selective affinity for muscarinic cholinergic receptors (*22*), caused no changes in the regional uptake. Similar negative results were observed for mice treated with mecamylamine, a noncompetitive nicotinic antagonist (*4*). None of the compounds tested had an effect on the radioactivity in the blood.

TABLE 2
Biodistribution of Radioactivity After Administration of ^{11}C-5MA

Biodistribution	Time after injection (min)				
	2	5	15	30	60
Blood	1.73 ± 0.35	1.35 ± 0.02	1.09 ± 0.06	0.83 ± 0.11	0.42 ± 0.02
Intestine	3.08 ± 0.58	3.22 ± 0.56	2.47 ± 0.13	2.44 ± 0.34	1.90 ± 0.39
Liver	7.29 ± 1.30	7.80 ± 0.36	5.53 ± 0.33	4.09 ± 0.52	2.34 ± 0.24
Kidney	20.0 ± 3.99	18.2 ± 0.19	21.6 ± 4.21	6.94 ± 1.09	4.88 ± 0.93
Stomach	2.01 ± 0.17	2.79 ± 0.34	2.56 ± 0.13	3.52 ± 0.52	2.19 ± 1.00
Spleen	3.31 ± 0.68	5.46 ± 0.97	4.28 ± 0.52	4.14 ± 1.83	1.57 ± 0.82
Pancreas	7.77 ± 1.08	7.00 ± 1.23	3.30 ± 0.12	1.93 ± 0.22	0.88 ± 0.24
Heart	4.87 ± 1.60	2.94 ± 0.51	1.53 ± 0.21	1.12 ± 0.30	0.62 ± 0.34
Lung	7.14 ± 2.46	5.78 ± 0.78	2.42 ± 0.46	1.54 ± 0.29	0.94 ± 0.32
Brain	1.23 ± 0.12	1.66 ± 0.09	2.24 ± 0.12	2.19 ± 0.24	1.87 ± 0.21
Br/Bl*	0.71 ± 0.15	1.23 ± 0.07	2.06 ± 0.19	2.65 ± 0.23	4.28 ± 0.46

*Br/Bl = brain-to-blood ratio (percentage of injected ^{11}C dose/gram of organ ratio).
Biodistribution of radioactivity is expressed as percentage of injected ^{11}C dose/gram of organ (mean ± SD for 4 mice).

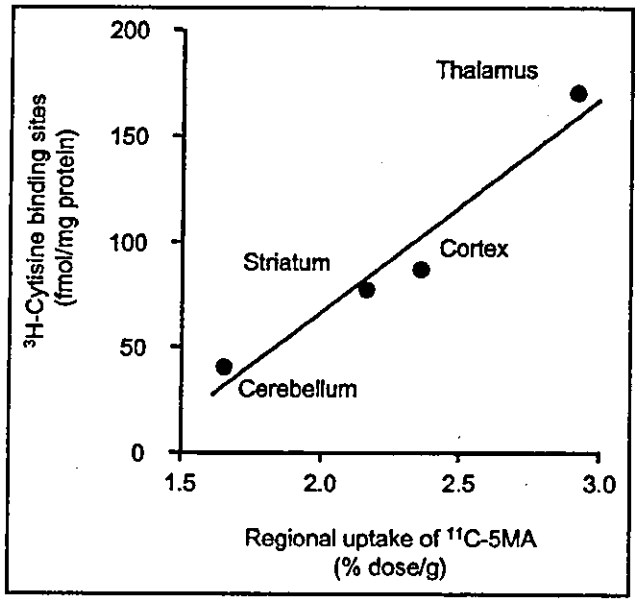

FIGURE 4. Correlation between radioactivity levels determined from in vivo distribution of ^{11}C-5MA and density of nicotinic cholinergic receptor sites as determined by in vitro (−)-^{3}H-cytisine binding (*35*).

The analysis of brain homogenates was performed at 30 min after injection of ^{11}C-5MA. Approximately 90% of the radioactivity in the homogenate could be extracted with methanol. No radioactive metabolites were observed in the brain homogenates, indicating that the cerebral accumulation of radioactivity occurred in the intact form.

PET Study of ^{11}C-5MA in Rhesus Monkey

A PET imaging study with ^{11}C-5MA in a rhesus monkey demonstrated high uptake and a noticeably heterogeneous distribution of radioactivity in the brain. Figure 6A shows a PET image of ^{11}C-5MA in monkey brain slices at 60–90 min after injection. A high accumulation of radioactivity was observed in the thalamus. Figure 6B shows the effect of (−)-cytisine on the cerebral distribution of ^{11}C-5MA. Treatment with (−)-cytisine 90 min before injection of the radioligand reduced the accumulation of radioactivity in regions of high uptake in the untreated experiment and resulted in nearly identical levels of radioactivity in all regions. Figure 7 shows time–radioactivity curves in the thalamus and cerebellum after intravenous injection of ^{11}C-5MA. After injection of ^{11}C-5MA, the radioactivity was rapidly taken up by the brain. Thereafter, the radioactivity in the thalamus increased further with time and then remained constant after 50 min, whereas that in the cerebellum was constant at 5–30 min and then decreased gradually with

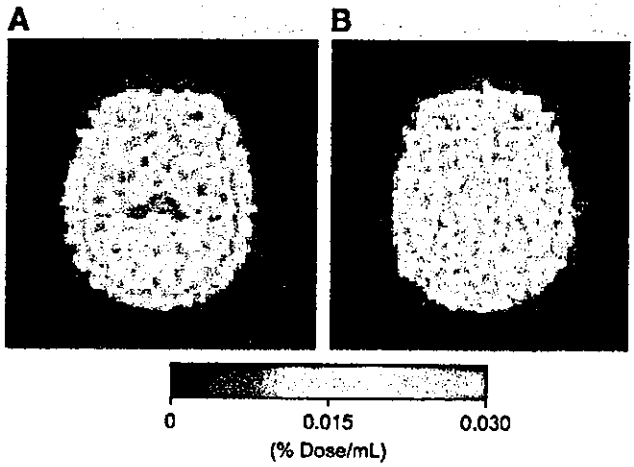

FIGURE 6. Transaxial PET images at 60–90 min after injection of ^{11}C-5MA in rhesus monkey. (A) ^{11}C-5MA alone. (B) (−)-Cytisine (5 mg/kg) administered 90 min before ^{11}C-5MA injection.

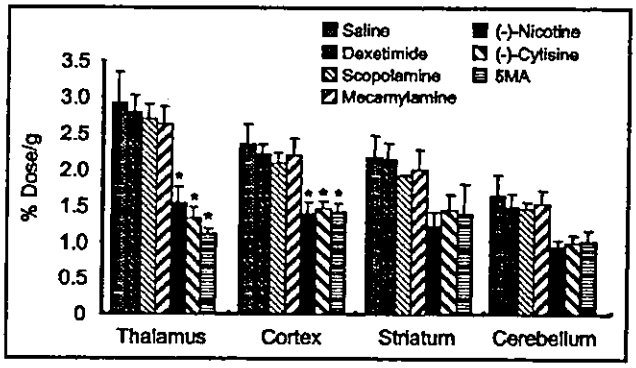

FIGURE 5. Effect of various drugs on regional uptake of ^{11}C-5MA in mice 30 min after injection. ^{11}C-5MA was intravenously injected 5 min after intravenous administration of (−)-cytisine (1 mg/kg), (−)-nicotine (60 μg/kg), dexetimide (10 mg/kg), 5MA (0.1 mg/kg), and saline and 30 min after subcutaneous administration of scopolamine (10 mg/kg) and mecamylamine (5 mg/kg). Data are presented as mean ± SD. *$P < 0.01$ as compared with saline control group (Dunnett multiple comparisons test).

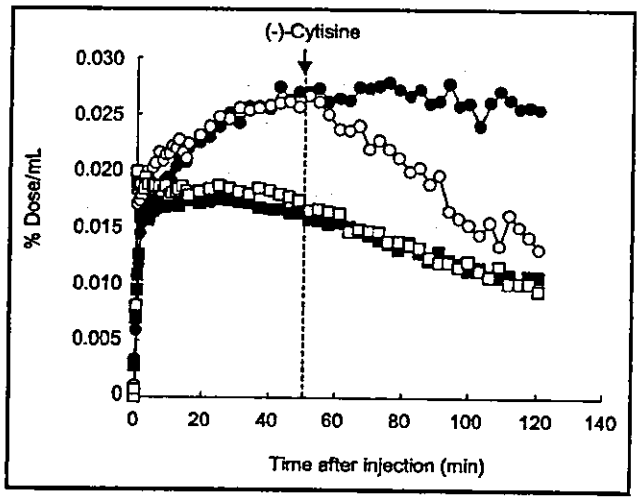

FIGURE 7. Time–radioactivity curves of ^{11}C-5MA in rhesus monkey. (−)-Cytisine (5.0 mg/kg) was intravenously administered 50 min after ^{11}C-5MA injection. ●, Thalamus in control study; ■, cerebellum in control study; ○, thalamus in (−)-cytisine displacement study; □, cerebellum in (−)-cytisine displacement study.

time after approximately 30 min. The treatment with (−)-cytisine (5 mg/kg, intravenous) 50 min after injection of the radioligand rapidly reduced the radioactivity in the thalamus, resulting in nearly the same level of radioactivity as that in the cerebellum 50 min after (−)-cytisine administration. In contrast, no change in the level of radioactivity was observed in the cerebellum on treatment with (−)-cytisine. The level of radioactivity in the blood was not significantly different after (−)-cytisine treatment.

DISCUSSION

The basic requirements for the effective use of radioligands for in vivo studies of central nAChRs include high affinity and selectivity for the receptors, quantitatively significant brain uptake after peripheral administration, and a regional cerebral distribution that is well correlated with the nAChR density of a site (*12*).

Since 5IA, an A-85380 analog iodinated at the 5-position of the pyridine ring, showed high affinity for nAChRs without a disturbance of receptor binding (*12,21,28,37*), it has been suggested that position 5 of the pyridyl fragment is the appropriate site for introduction of the ^{11}C-methyl group in A-85380. In fact, Holladay et al. recently found that 5MA has high affinity for nAChRs (*28*). Our study on the receptor-binding assay also confirmed high affinity of 5MA for nAChRs—that is, 5MA has approximately 1.5 times higher affinity than A-85380, 3.5 times higher affinity than (−)-cytisine, and 10 times higher affinity than (−)-nicotine (Fig. 2; Table 1). Thus, the results indicate that position 5 is a suitable site for introduction of the methyl group in the A-85380 molecule.

In vivo biodistribution studies with ^{11}C-5MA showed high accumulation in the brain. The radioactivity in the brain increased with time after injection and the peak level was reached at 15 min, showing an increase by a factor of 1.8 compared with that at 2 min (Table 2). The slightly slow uptake kinetics of ^{11}C-5MA by the brain may be responsible for the moderate BUI.

Studies on the regional brain distribution showed that 5MA had high accumulation of radioactivity in the thalamus, intermediate accumulation in the cortex, striatum, and hippocampus, and low accumulation in the cerebellum (Fig. 3). This regional distribution correlated well with the known distribution of nAChRs (*35*) (Fig. 4). In addition, the administration of (−)-cytisine and (−)-nicotine, nAChR-binding agents (*13,18,28,30,36*), reduced the uptake of radioactivity at higher magnitude in regions of higher uptake in the untreated brain and resulted in almost the same level throughout the brain. However, dexetimide, scopolamine, and mecamylamine did not influence the cerebral distribution of ^{11}C-5MA. These results indicate the selective binding of ^{11}C-5MA to nAChRs in the brain. Furthermore, injection of nonradioactive 5MA (0.1 mg/kg) resulted in a marked reduction in the uptake of radioactivity in the brain. This finding demonstrated the saturability of the sites labeled with ^{11}C-5MA. These results on selectivity and saturability indicated that ^{11}C-5MA binds to nAChRs in the brain after intravenous injection.

Imaging studies with PET in rhesus monkey demonstrated that ^{11}C-5MA can be used to visualize nAChRs in the brain. Furthermore, ^{11}C-5MA uptake was displaced by treatment with (−)-cytisine, showing that the binding of ^{11}C-5MA to nAChR sites was reversible.

When the in vivo behavior of ^{11}C-5MA in the mouse brain was compared with previously published data on other A85380 derivatives labeled with a positron radionuclide, 2-^{18}F-fluoro-A-85380 (2-^{18}F-FA) and 6-^{18}F-fluoro-A-85380 (6-^{18}F-FA) (*38,39*), the total uptake and the thalamus-to-cerebellum ratio, target-to-nontarget ratio, of ^{11}C-5MA in the mouse brain were lower than those of 2-^{18}F-FA and 6-^{18}F-FA. On the other hand, the uptake rate of ^{11}C-5MA by the thalamus was comparable with that of 2-^{18}F-FA and faster than that of 6-^{18}F-FA, and clearance of ^{11}C-5MA from the thalamus was faster than 6-^{18}F-FA and slower than 2-^{18}F-FA. However, with regard to the accumulation and clearance in the thalamus, it has been reported that, in the baboon, 6-^{18}F-FA exhibited faster accumulation followed by a faster decline compared with that of 2-^{18}F-FA, as opposed to the data in mice (*40*). Thus, although a high uptake and target-to-nontarget ratio of 2-^{18}F-FA and 6-^{18}F-FA in the mouse brain may be preferable to ^{11}C-5MA, further comparative studies are required on cerebral behavior of the 3 radioligands in other animals.

In addition, displacement studies of ^{11}C-5MA showed that some radioactivity remained in the brain after treatment with (−)-nicotine and (−)-cytisine. Although the cause of this finding is unclear, it may be due to high nonspecific binding or a large amount of free ligand in the brain. In this study, the timing of the displacement studies (30 min) may have been too early to remove completely free ligands from the brain because the radioactivity in the cerebellum declined further with time after 30 min (Fig. 3). More studies are required of this high residual uptake.

CONCLUSION

In this study, ^{11}C-5MA, an A-85380 derivative ^{11}C-methylated at position 5 of the pyridyl fragment, was synthesized by rapid ^{11}C-methylation using ^{11}C-methyl iodide. In vitro competitive binding studies showed high affinity of 5MA for brain nAChRs. In vivo biodistribution studies demonstrated that ^{11}C-5MA showed high brain uptake and regional cerebral distribution in association with nAChRs after intravenous injection. Furthermore, ^{11}C-5MA allowed visualization of central nAChR sites in the rhesus monkey by PET. Thus, ^{11}C-5MA is a potential radioligand for use in PET investigations of central nAChRs in humans.

ACKNOWLEDGMENTS

This work was supported in part by a grant from the Research for the Future Program of the Japan Society for

the Promotion of Science (JSPS-RFTF97K00201); grants-in-aid for Scientific Research from the Ministry of Education, Culture, Sports, Science and Technology of Japan; a grant-in-aid for Creative Scientific Research of the Japan Society for the Promotion of Science; and a grant from the Smoking Research Foundation.

REFERENCES

1 Irle E, Markowitsch HJ. Basal forebrain-lesioned monkeys are severely impaired in tasks of association and recognition memory. *Ann Neurol.* 1987;22:735–743.
2 Decker MW, Brioni JD, Bannon AW, Arneric SP. Diversity of neuronal nicotinic acetylcholine receptors: lessons from behavior and implications for CNS therapeutics. *Life Sci.* 1995;56:545–570.
3 White HK, Levin ED. Four-week nicotine skin patch treatment effects on cognitive performance in Alzheimer's disease. *Psychopharmacology (Berl).* 1999;143:158–165.
4 Paterson D, Nordberg A. Neuronal nicotinic receptors in the human brain. *Prog Neurobiol.* 2000;61:75–111.
5 Nordberg A, Alafuzoff I, Winblad B. Nicotinic and muscarinic subtypes in the human brain: changes with aging and dementia. *J Neurosci Res.* 1992;31:103–111.
6 Flynn DD, Mash DC. Characterization of L-[^{3}H]nicotine binding in human cerebral cortex: comparison between Alzheimer's disease and the normal. *J Neurochem.* 1986;47:1948–1954.
7 London ED, Ball MJ, Waller SB. Nicotinic binding sites in cerebral cortex and hippocampus in Alzheimer's dementia. *Neurochem Res.* 1989;14:745–750.
8 Silver W, Gillberg PG, Svensson AL, Nordberg A. Autoradiographic comparison of [^{3}H](−)-nicotine, [^{3}H]cytisine and [^{3}H]epibatidine binding in relation to vesicular acetylcholine transport sites in the temporal cortex in Alzheimer's disease. *Neuroscience.* 1999;94:685–696.
9 Whitehouse PJ, Martino AM, Wagster MV, et al. Reductions in [^{3}H]nicotine acetylcholine binding in Alzheimer's disease and Parkinson's disease: an autoradiographic study. *Neurology.* 1988;38:720–723.
10 Perry EK, Morris CM, Court JA, et al. Alteration in nicotine binding sites in Parkinson's disease, Lewy body dementia and Alzheimer's disease: possible index of early neuropathology. *Neuroscience.* 1995;64:385–395.
11 Perry DC, Davila-Garcia MI, Stockmeier CA, Kellar KJ. Increased nicotinic receptors in brains from smokers: membrane binding and autoradiography studies. *J Pharmacol Exp Ther.* 1999;289:1545–1552.
12 Silver W, Nordberg A, Langstrom B, et al. Development of ligands for *in vivo* imaging of cerebral nicotinic receptors. *Behav Brain Res.* 2000;113:143–157.
13 Nyback H, Halldin C, Ahlin A, et al. PET studies of the uptake of (S)- and (R)-[^{11}C]nicotine in the human brain: difficulties in visualizing specific receptor binding *in vivo*. *Psychopharmacology (Berl).* 1994;115:31–36.
14 Saji H, Watanabe A, Magata Y, et al. Synthesis and characterization of radioiodinated (S)-5-iodonicotine: a new ligand for potential imaging of brain nicotinic cholinergic receptors by single photon emission computed tomography. *Chem Pharm Bull.* 1997;45:284–290.
15 Horti A, Scheffel U, Stathis M, et al. Fluorine-18-FPH for PET imaging of nicotinic acetylcholine receptors. *J Nucl Med.* 1997;38:1260–1265.
16 Ding YS, Molina PE, Fowler JS, et al. Comparative studies of epibatidine derivatives [^{18}F]NFEP and [^{18}F]N-methyl-NFEP: kinetics, nicotine effect, and toxicity. *Nucl Med Biol.* 1999;26:139–148.
17 Sullivan JP, Donnelly-Roberts D, Briggs CA, et al. A-85380 [3-(2(S)-azetidinylmethoxy) pyridine]: *in vitro* pharmacological properties of a novel, high affinity alpha 4 beta 2 nicotinic acetylcholine receptor ligand. *Neuropharmacology.* 1996;35:725–734.
18 Abreo MA, Lin NH, Garvey DS, et al. Novel 3-pyridyl ethers with subnanomolar affinity for central neuronal nicotinic acetylcholine receptors. *J Med Chem.* 1996;39:817–825.
19 Valette H, Bottlaender M, Dolle F, et al. Imaging central nicotinic acetylcholine receptors in baboons with [^{18}F]fluoro-A-85380. *J Nucl Med.* 1999;40:1374–1380.
20 Horti AG, Chefer SI, Mukhin AG, et al. 6-[^{18}F]Fluoro-A-85380, a novel radioligand for *in vivo* imaging of central nicotinic acetylcholine receptors. *Life Sci.* 2000;67:463–469.
21 Koren AO, Horti AG, Mukhin AG, et al. 2-, 5-, and 6-Halo-3-(2(S)-azetidinylmethoxy)pyridines: synthesis, affinity for nicotinic acetylcholine receptors, and molecular modeling. *J Med Chem.* 1998;41:3690–3698.
22 Vaupel DB, Mukhin AG, Kimes AS, Horti AG, Koren AO, London ED. In vivo studies with [^{125}I]-5-I-A-85380, a nicotinic acetylcholine receptor radioligand. *Neuroreport.* 1998;9:2311–2317.
23 Musachio JL, Scheffel U, Finley PA, et al. 5-[I-125 123]Iodo-3(2(S)-azetidinylmethoxy)pyridine, a radioiodinated analog of A-85380 for in vivo studies of central nicotinic acetylcholine receptors. *Life Sci.* 1998;62:351–357.
24 Chefer SI, Horti AG, Lee KS, et al. In vivo imaging of brain nicotinic acetylcholine receptors with 5-[^{123}I]iodo-A-85380 using single photon emission computed tomography. *Life Sci.* 1998;63:355–360.
25 Musachio JL, Villemagne VL, Scheffel UA, et al. Synthesis of an I-123 analog of A-85380 and preliminary SPECT imaging of nicotinic receptors in baboon. *Nucl Med Biol.* 1999;26:201–207.
26 Fujita M, Tamagnan G, Zoghbi SS, et al. Measurement of $\alpha_4\beta_2$ nicotinic acetylcholine receptors with [I-123]5-I-A-85380 SPECT. *J Nucl Med.* 2000;41:1552–1560.
27 Saji H, Ogawa M, Ueda M, et al. Evaluation of radioiodinated 5-iodo-3-(2(S)-azetidinylmethoxy)pyridine as a ligand for SPECT investigations of brain nicotinic acetylcholine receptors. *Ann Nucl Med.* 2002;16:189–200.
28 Holladay MW, Bai H, Li Y, et al. Structure-activity studies related to ABT-594, a potent nonopioid analgesic agent: effect of pyridine and azetidine ring substitutions on nicotinic acetylcholine receptor binding affinity and analgesic activity in mice. *Bioorg Med Chem Lett.* 1998;8:2797–2802.
29 Karimi F, Langstrom B. Synthesis of 3-[(2*S*)-azetidin-2-ylmethoxy]-5-[^{11}C]-methylpyridine, an analogue of A-85380, via a Still coupling. *J Labelled Compds Radiopharm.* 2002;45:423–434.
30 Pabreza LA, Dhawan S, Kellar KJ. [^{3}H]Cytisine binding to nicotinic cholinergic receptors in brain. *Mol Pharmacol.* 1991;39:9–12.
31 Oldendorf WH. Measurement of brain uptake of radiolabeled substances using a tritiated water internal standard. *Brain Res.* 1970;24:372–376.
32 Magata Y, Saji H, Choi SR, et al. Noninvasive measurement of cerebral blood flow and glucose metabolic rate in the rat with high-resolution animal positron emission tomography (PET): a novel *in vivo* approach for assessing drug action in the brains of small animals. *Biol Pharm Bull.* 1995;18:753–756.
33 Tsukada H, Harada N, Nishiyama S, et al. Ketamine decreased striatal [^{11}C]raclopride binding with no alterations in static dopamine concentrations in the striatal extracellular fluid in the monkey brain: multiparametric PET studies combined with microdialysis analysis. *Synapse.* 2000;37:95–103.
34 Suzuki M, Doi H, Bjorkman M, et al. Rapid coupling of methyl iodide with aryltributylstannanes mediated by palladium(0) complexes: a general protocol for the synthesis of ^{11}C-labeled PET tracers. *Chem Eur J.* 1997;3:2039–2041.
35 Sargent PB. The diversity of neuronal nicotinic acetylcholine receptors. *Annu Rev Neurosci.* 1993;16:403–443.
36 Flesher JE, Scheffel U, London ED, Frost JJ. In vivo labeling of nicotinic cholinergic receptors in the brain with [^{3}H]cytisine. *Life Sci.* 1994;54:1883–1890.
37 Mukhin AG, Gundisch D, Horti AG, et al. 5-Iodo-A-85380, an $\alpha_4\beta_2$ subtype-selective ligand for nicotinic acetylcholine receptors. *Mol Pharmacol.* 2000;57:642–649.
38 Horti AG, Scheffel U, Koren AO, et al. 2-[^{18}F]Fluoro-A-85380, an in vivo tracer for the nicotinic acetylcholine receptors. *Nucl Med Biol.* 1998;25:599–603.
39 Scheffel U, Horti AG, Koren AO, et al. 6-[^{18}F]Fluoro-A-85380: an in vivo tracer for the nicotinic acetylcholine receptors. *Nucl Med Biol.* 2000;27:51–56.
40 Ding YS, Wang T, Marecek J, et al. Synthesis and evaluation of 6-[^{18}F]fluoro-3-(2(S)-azetidinylmethoxy)pyridine as a PET tracer for nicotinic acetylcholine receptors. *Nucl Med Biol.* 2000;27:381–389.

ELSEVIER

NeuroImage

www.elsevier.com/locate/ynimg
NeuroImage 22 (2004) 553–561

Cognitive- and motor-related regions in Parkinson's disease: FDOPA and FDG PET studies

Atsuko Nagano-Saito,[a,b,c,*] Takashi Kato,[a] Yutaka Arahata,[b] Yukihiko Washimi,[b] Akinori Nakamura,[a] Yuji Abe,[b] Takako Yamada,[b] Katsushige Iwai,[b] Kentaro Hatano,[a] Yasuhiro Kawasumi,[a] Teruhiko Kachi,[b] Alain Dagher,[c] and Kengo Ito[a]

[a] *Department of Biofunctional Research, National Institute for Longevity Sciences, Obu, Japan*
[b] *Department of Neurology, Chubu National Hospital, Obu, Japan*
[c] *McConnell Brain Imaging Centre, Montreal Neurological Institute, McGill University, Montreal, Canada*

Received 25 June 2003; revised 18 December 2003; accepted 16 January 2004

Available online 1 April 2004

Objective: **Using 6-[^{18}F]fluoro-L-dopa (FDOPA) and [^{18}F]fluorodeoxyglucoce (FDG) positron emission tomography (PET), multiple regression analyses were performed to determine the specific brain regions that are related to cognitive and motor symptoms in nondemented patients with Parkinson's disease.** *Methods:* **Spatially normalized images of FDOPA influx rate constant (Ki) values and relative regional cerebral metabolic rates for glucose (rrCMRglc) were created. Raven's Coloured Progressive Matrices (RCPM) scores and the Unified Parkinson's Disease Rating Scale (UPDRS) motor scores were used to determine the patients' cognitive and motor functions, respectively. Multiple correlation analyses between the FDOPA and FDG images and the cognitive and motor scores were performed for each voxel.** *Results:* **RCPM score was significantly positively correlated with the FDOPA Ki in the left hippocampus and with the rrCMRglc in the left middle frontal gyrus and right retrosplenial cortex. Motor function was significantly positively correlated with the FDOPA Ki in the bilateral striatum and with the rrCMRglc in association areas and primary visual cortex. The level of motor function was significantly inversely correlated with the FDOPA Ki in the anterior cingulate gyrus and with the rrCMRglc in bilateral primary motor cortex and right putamen.** *Conclusions:* **Changes of striatal FDOPA uptake and rrCMRglc in the primary motor cortex likely represent dysfunction in the motor system involving the corticobasal ganglia-thalamocortical loop. Change of FDOPA uptake in the anterior cingulate gyrus may be related to up-regulation of dopamine synthesis in surviving dopamine neurons. The regions where correlation with cognitive function was observed belong to a cognitive frontoparietal–hippocampal network.**

Keywords: Parkinson's disease; Positron emission tomography; 6-[^{18}F]fluoro-L-dopa; [^{18}F]fluorodeoxyglucoce

Introduction

Parkinson's disease (PD) is a progressive degenerative disorder characterized clinically by tremor, rigidity, and bradykinesia and pathologically by dopamine deficiency in the striatum. Cognitive impairment is also a common symptom observed among PD patients, especially at an advanced stage. The prevalence rate of dementia is estimated at 20–40% of PD patients (Aarsland et al., 1996; Giladi et al., 2000), and even in PD patients without dementia, specific impairments in executive function, visual memory, and/or visuospatial abilities are prevalent (Dubois and Pillon, 1997; Janvin et al., 2003).

The target cells of the projection from the dopaminergic neurons in the substantia nigra are located in the striatum, a component of parallel corticobasal ganglia-thalamocortical (CBGTC) loops. This neural system includes functionally distinct loops, including a "motor loop," and an "associative loop," which is involved in cognitive functions. At the level of the striatum, the motor loop is largely centered on the putamen and the associative loop mostly on the caudate (Alexander et al., 1986; Middleton and Strick, 1996; Parent and Hazrati, 1995).

6-[^{18}F]fluoro-L-dopa (FDOPA) positron emission tomography (PET) has been used to investigate the activity of aromatic L-amino acid decarboxylase in the striatum and to assess the integrity of the dopaminergic system in vivo (Garnett et al., 1983). In patients with PD, FDOPA uptake in the striatum is decreased (Brooks et al., 1990; Garnett et al., 1984; Nahmias et al., 1985) and there is an inverse correlation between the degree of motor deficit and FDOPA uptake in the striatum, especially in the putamen (Holthoff-Detto et al., 1997; Leenders et al., 1990; Rinne et al., 2000; Vingerhoets et al., 1997). Meanwhile, correlations between FDOPA uptake in the caudate and cognitive function have been shown in groups of demented and nondemented PD patients (Ito et al., 2002; Rinne et al., 2000). In nondemented PD patients, there have been reports of a positive correlation between FDOPA uptake in the caudate and memory performance (Holthoff-Detto et al., 1997) and impairment of tactile object discrimination in patients with low caudal dopaminergic function (Weder et al., 1999). The findings of these

* Corresponding author. Department of Biofunctional Research, National Institute for Longevity Sciences, 36-3 Gengo, Morioka, Obu, Aichi Prefecture, 474-8522, Japan. Fax: +81-562-44-6596.
E-mail addresses: anagano@sannet.ne.jp, atsuko@bic.mni.mcgill.ca (A. Nagano-Saito).
Available online on ScienceDirect (www.sciencedirect.com.)

1053-8119/$ - see front matter © 2004 Published by Elsevier Inc.
doi:10.1016/j.neuroimage.2004.01.030

FDOPA PET studies are consistent with the parallel CBGTC loop model. However, the following findings are less consistent with this model: no correlation between FDOPA uptake in the caudate and cognitive functions (Broussolle et al., 1999), a relationship between motor function and FDOPA uptake in the caudate, as well as in the putamen (Brooks et al., 1990; Broussolle et al., 1999; Vingerhoets et al., 1997), and a correlation between a cognitive function and the FDOPA uptake in the putamen (Holthoff et al., 1994).

The results of measurement of local cerebral metabolic rate for glucose in the resting state using [^{18}F]fluorodeoxyglucoce (FDG) PET (Phelps et al., 1979) are more complex. Because the main output target of the basal ganglia is the frontal lobe, frontal hypometabolism might have been predicted (Carbon and Marie, 2003). However, it is the parietal cortex that displays hypometabolism in PD patients, a finding that has been frequently linked to the presence of dementia (Karbe et al., 1992; Kuhl et al., 1984; Peppard et al., 1992; Piert et al., 1996). Moreover, even in non-demented PD patients, parietal hypometabolism compared to normal controls has been frequently reported (Arahata et al., 1999; Bohnen et al., 1999; Eberling et al., 1994; Hu et al., 2000; Peppard et al., 1992; Piert et al., 1996). In addition, positive correlations between parietal hypometabolism and motor dysfunction (Eidelberg et al., 1994; Moeller and Eidelberg, 1997) and cognitive impairment (Mentis et al., 2002; Wu et al., 2000) have also been observed.

These results indicate that FDOPA uptake both in the putamen and the caudate nucleus and parietal hypometabolism may both be related to motor and, in some cases, cognitive function may be attributed to parallel progression of motor and cognitive damage in PD patients. Alternatively, the same neural population in the caudate, putamen, and parietal area may subserve both cognitive and motor function in PD patients. Whether parietal hypometabolism is related to impairment of nigrostriatal dopaminergic system or to alternative neuropathological processes that occur relatively parallel with but not perfectly simultaneously to the impairment in PD is unclear. To clarify these points, we undertook a double tracer study with FDOPA and FDG PET in the same group of PD patients.

We employed FDOPA PET, FDG PET, and multiple regression analysis using measures of cognitive and motor function in the same PD patients. To avoid using a priori regions of interest (ROI), SPM99 (Friston et al., 1995) was used for these analyses. Motor function was assessed with the Unified Parkinson's Disease Rating Scale (UPDRS) motor scores (Note: higher scores denote greater parkinsonian disability). Cognitive function was assessed with Raven's Coloured Progressive Matrices (RCPM) because it is sensitive to cognitive deficits in PD (Farina et al., 2000). This test was initially developed as a nonverbal intellectual test (Raven, 1962; Sugishita and Yamasaki, 1993) and can be considered to rely on at least two cognitive factors: visuospatial and executive functions. Higher RCPM scores indicate better performance, and performance does not correlate significantly with severity of PD motor symptoms (Cronin-Golomb and Braun, 1997).

Materials and methods

Subjects

Twenty-eight patients with PD (males 12, females 16; mean age ± SD: 62.6 ± 7.7 years; 12 with predominantly left PD signs, 15 with predominantly right PD signs, and 1 case with bilateral signs) were enrolled in this study. The mean duration of disease was 3.8 years (SD: 2.6 years; range: 1–10 years). All patients were examined by a neurologist at Chubu National Hospital and fulfilled the clinical criteria for the diagnosis of PD (Calne et al., 1992). The mean of the Hoehn and Yahr score (Hoehn and Yahr, 1967) was 2.5 (SD: 0.9), and 3 three patients were in stage I, 11 in stage II, 9 in stage III, and 5 in stage IV. Patients underwent neuropsychological assessment to exclude dementia or other mental impairments. Patients who fulfilled the Diagnostic and Statistical Manual of Mental Disorders (DSM) IV criteria for either delirium, dementia, or an amnestic disorder or alternatively the consortium on dementia with Lewy bodies international workshop criteria (McKeith et al., 1996) were excluded. General dementia severity was measured by the Mini-Mental State Examination (MMSE) (Folstein et al., 1975), and the patients whose MMSE scores were less than 24 were also excluded. The mean MMSE score was 28.5 (SD: 1.6; range: 25–30). Patients with hallucination episodes, severe depression, severe autonomic failure, or resistance to dopaminergic agonists were also excluded, and all of our patients' scores for questions 1 (intellectual impairment), 2 (thought disorder), and 3 (depression) of the UPDRS were 0 or 1. Each patient was assessed clinically by a neurologist before their PET study and at least 24 h after discontinuing their medications for PD.

Permission to perform these studies was obtained from the Ethical Committee of Chubu National Hospital. All of the patients and normal subjects gave written informed consents before PET scanning.

Data acquisition and analysis

FDOPA PET

An oral dose (100 mg) of carbidopa, a peripheral aromatic amino acid decarboxylase inhibitor, was given 1 h before PET scanning. Dynamic FDOPA PET studies were performed using an ECAT EXACT HR47 (CTI/Siemens, Knoxville, TN) in three-dimensional acquisition mode, which yielded 47 simultaneous planes, with an axial full-width half-maximum (FWHM) resolution of 4.8 mm and an in-plane resolution of 4.0 × 3.9 mm at the center. A mold made of an air cushion was fitted to minimize head movement. The subject was positioned in the scanner so that the entire brain was within the field of view. For correction of tissue attenuation of 511 keV annihilation radiation, a 10-min, two-dimensional transmission scan was performed before tracer injection using a retractable 68Ga/68Ge source.

Eighty to 180 MBq of FDOPA was infused intravenously into each subject over 30 s. Scanning began at the start of tracer injection. The protocol included 25 time frames (4 × 1, 3 × 2, 3 × 3, and 15 × 5 min) over 94 min.

Data analysis was performed on a Sun workstation (Sun Microsysytems, Silicon Valley, CA). The dynamic FDOPA PET data of the subjects who displayed significant head movements between scans were realigned using the alignment program in SPM99. For each subject, an FDOPA Ki image and an FDOPA add image were generated on a voxel-by-voxel basis from the dynamic FDOPA PET data. These images were generated using the analysis software, 'kronos,' which was written by Dale Bailey (MRC Cyclotron Unit, Hammersmith Hospital, London, UK) using IDL Image Analysis software (Research Systems, Inc., Boulder, CO). The FDOPA Ki image was based on the multiple

time graphical analysis (MTGA) approach of Patlak and Blasberg (Martin et al., 1989; Patlak and Blasberg, 1985). We used the cerebellar tissue counts between 0 and 94 min postinjection as the input function and the count samples on a voxel-by-voxel basis between 24 and 94 min to draw the regression lines in MTGA. The right and left cerebellar regions of interests (ROIs) were placed on each of three adjacent slices. The FDOPA add image was created as an integrated image of the 14 late time frames (24–94 min).

For transformation into stereotaxic space, an FDOPA template was generated. First, the FDOPA add images of 13 normal volunteers that were used in our previous report (Nagano et al., 2000) were coregistered to their individual magnetic resonance image (MRI) by using coregistration software in SPM99. Individual MRIs were transformed into the standard stereotactic space using the normalization program in SPM99 with the Montreal Neurological Institute (MNI) template (Mazziotta et al., 1995). With the same transforming parameters, the add images were then transformed into the standard stereotactic space. These 13 transformed add images were averaged and the averaged image was smoothed with an isotropic Gaussian kernel (FWHM = 6 mm). This averaged smoothed FDOPA add image was used as the template image for this study. The subjects' FDOPA add images in this study were transformed into the standard stereotactic space using the template image. Then, the Ki images were transformed into standard stereotactic space using the same transformation. After normalization, the Ki images were smoothed with an isotropic Gaussian kernel (FWHM = 6 mm).

FDG PET

Fasting was required at least 4 h before the scans. FDG PET studies were performed in two-dimensional acquisition mode, which yielded 47 simultaneous planes, with an axial FWHM resolution of 4.1 mm and an in-plane resolution of 4.0 × 3.9 mm at the center. Three hundred to 370 MBq of FDG was infused intravenously into each subject over 120 s. The protocol included 18 time frames (12 × 2, 4 × 4, 2 × 10 min) over 60 min, and the summed image was obtained from the last three frames, namely, data from 36 to 60 min after injection.

The FDG summed images were directly transformed into the standard stereotactic space using the H_2O PET template in SPM. After spatial normalization, the images were smoothed with an isotropic Gaussian kernel (FWHM = 10 mm). To reduce the effect of intersubject variability of brain glucose metabolism (Wang et al., 1994), the smoothed images were globally normalized. The mean value of the voxels, whose counts were higher than 60% of the highest value and in which almost all of the cortex, thalamus, and striatum were included, was used for global normalization for each subject. The values in the globally normalized images were considered to approximate relative regional cerebral metabolic rate for glucose (rCMRglc) (Hutchins et al., 1984).

Statistical analysis

Multiple correlation analyses between both parametric images and the cognitive and motor scores were performed for each voxel using the general linear approach (Friston et al., 1995) in SPM99. The RCPM score and the UPDRS motor score were incorporated as covariates of interest. The effect of each comparison was tested and the result was indicated as a T map. Clusters with the height threshold set at $P < 0.01$ with extent threshold set at corrected $P < 0.05$ were considered significant. In addition to this, when the regions were consistent with previous studies or when the results of FDOPA and FDG studies implicated the same neuroanatomical system, voxels with threshold of uncorrected $P < 0.005$ were also considered as significant.

The limbic or paralimbic system, as well as the striatum, was included in our analysis of FDOPA PET data. In addition to the nigrostriatal system, there are mesolimbic system and mesocortical dopaminergic projections (Kretshmann and Weinirich, 1992), and we previously showed that it was possible to reliably estimate FDOPA uptake in the limbic or paralimbic system, such as the

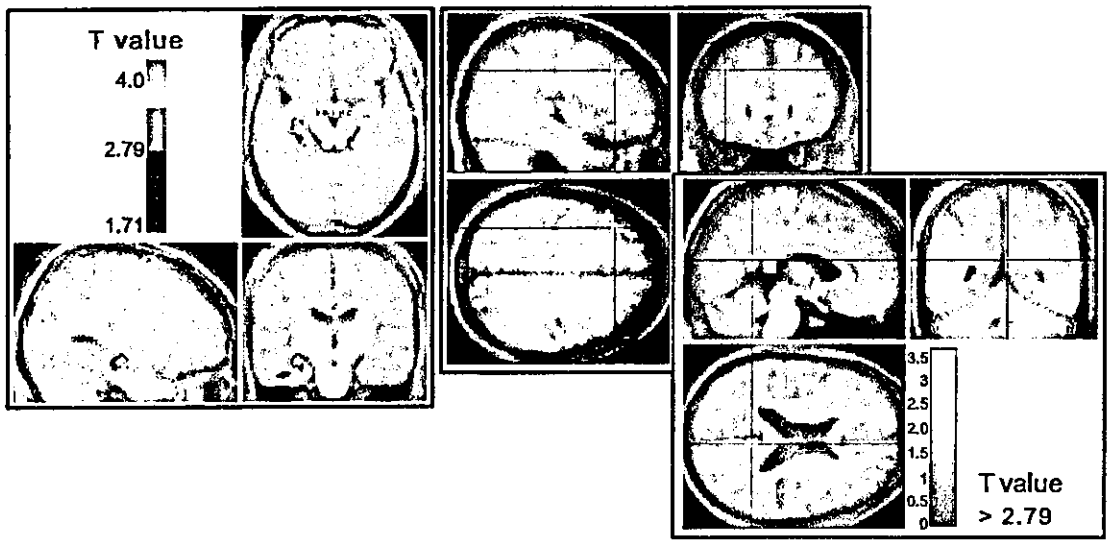

Fig. 1. Region with significantly positive correlation to the RCPM score in the FDOPA study (left) and in the FDG study (right). The T values 1.71 and 2.79 correspond the height threshold set at $P < 0.05$ and 0.005, respectively.

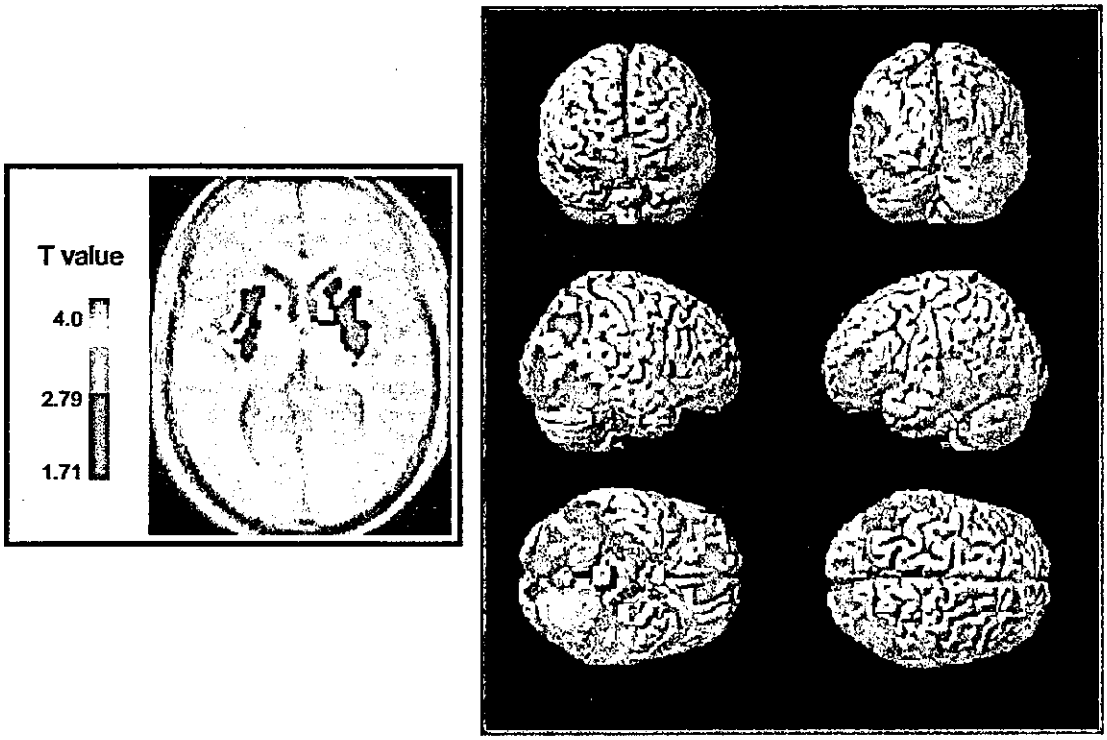

Fig. 2. Regions with significantly inverse correlation to the UPDRS motor score in the FDOPA study (left) and in the FDG study (right). The T values 1.71 and 2.79 correspond the height threshold set at $P < 0.05$ and 0.005, respectively.

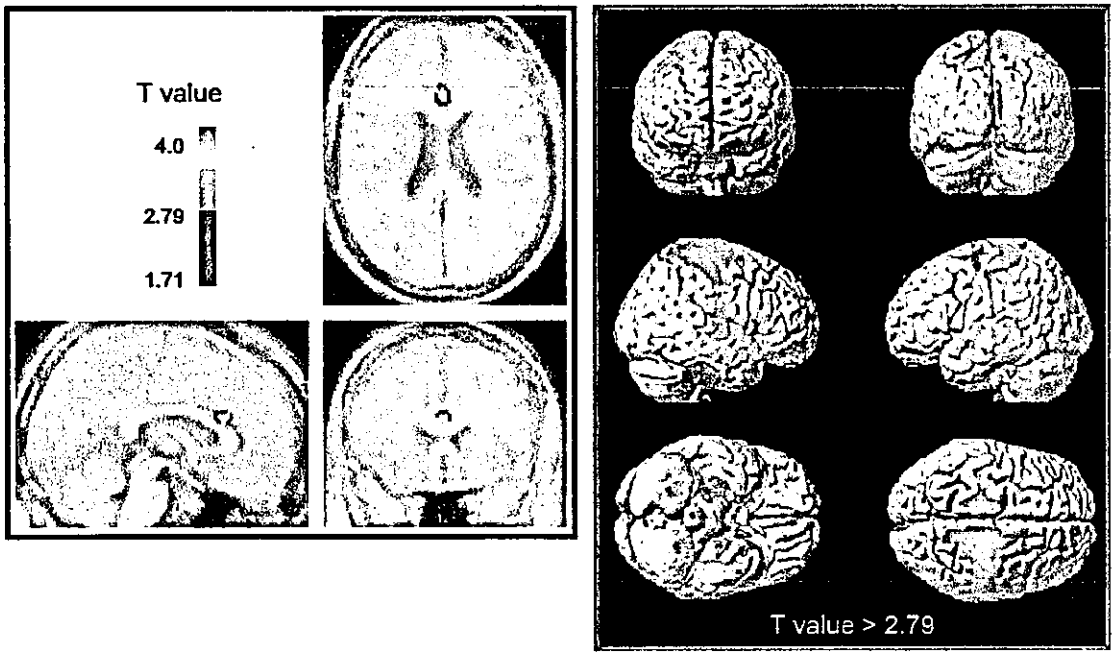

Fig. 3. Region with significantly positive correlation to the UPDRS motor score in the FDOPA study (left) and in the FDG study (right). The T values 1.71 and 2.79 correspond the height threshold set at $P < 0.05$ and 0.005, respectively.

hippocampus, amygdala, and anterior cingulate gyrus, in normal subjects (Nagano et al., 2000).

Results

The mean RCPM score was 30.4 (SD: 5.0; range: 21–36), and the mean UPDRS motor score was 29.2 (SD: 18.8; range: 5–65). There was no significant correlation between the UPDRS motor scores and the RCPM scores (correlation coefficient of these scores was −0.005, $P = 0.98$).

Correlations with cognitive function

With the voxel-level threshold, the RCPM score was significantly positively correlated with the FDOPA Ki value in the left hippocampus and with rrCMRglc in the dorsolateral prefrontal cortex (left middle frontal gyrus, BA 9/46) and in the right retrosplenial cortex extending to the adjacent posterior cingulate gyrus (BA 29/30/23) (Fig. 1). There were no significantly inverse correlations between RCPM score and the FDOPA or FDG values.

Correlations with motor function

With the cluster-level threshold, the UPDRS motor score was significantly inversely correlated with the FDOPA Ki value in the bilateral striatum and with the rrCMRglc in bilateral lateral occipitotemporal area (BA 37). In addition to this, with the voxel-level threshold, the UPDRS motor score was significantly inversely correlated with rrCMRglc in the bilateral orbitofrontal gyrus (BA 11) extending to the anterior cingulate gyrus (BA 32), the bilateral primary and associative visual cortex (BA 17/18/19), the left middle frontal gyrus (BA 10) extending to the inferior frontal gyrus (BA 47), the right inferior parietal gyrus (BA 39/40), and the right middle frontal gyrus (BA 9/8) (Fig. 2).

With the cluster-level threshold, the UPDRS motor score was significantly positively correlated with the rrCMRglc in the right precentral gyrus (BA 4) (with the right side extending to the postcentral gyrus, BA 3/1/2). In addition to this, with the voxel-level threshold, the UPDRS motor score was significantly positively correlated with the FDOPA Ki value in the anterior cingulate gyrus (BA 24) and with rrCMRglc in the left precentral gyrus (BA 4), the right side of the middle frontal gyrus (BA 6), and the right putamen (Fig. 3).

Table 1
List of the peaks of the most significant correlations with RCPM and UPDRS motor scores in the FDOPA study

	Cluster level	Voxel level		x	y	z
	P corrected	*T*	*P* uncorrected			
RCPM positive						
lt hippocampus	0.096	3.98	<0.001	−30	−18	−16
lt island	0.935	3.15	0.002	−40	6	−16
UPDRS motor negative						
rt putamen	<0.001	3.62	0.001	12	8	−4
lt putamen	0.573	3.28	0.002	−34	−6	6
UPDR motor positive						
anterior cingulate gyrus	0.667	3.46	0.001	0	24	22

Abbreviations: lt = left; rt = right.

Table 2
List of the peaks of the most significant correlations with RCPM and UPDRS motor scores in the FDG study

	Cluster level	Voxel level		x	y	z
	P corrected	*T*	*P* uncorrected			
RCPM positive						
lt GFm BA 9	0.843	3.69	0.001	−38	30	38
rt GC BA 30	0.77	3.55	0.001	4	−52	18
UPDRS motor negative						
rt GTm BA 37	0.008	5.91	<0.001	56	−64	−14
lt GFm BA 10	0.030	4.85	<0.001	−40	52	−2
rt GFm BA 9	0.696	4.63	<0.001	42	4	32
rt LPi BA 39	0.014	4.49	<0.001	40	−60	40
lt GTi BA 37	<0.001	4.25	<0.001	−52	−46	−14
rt Gob BA 11	0.006	4.07	<0.001	16	50	−20
rt Cu BA 18	0.096	3.97	<0.001	8	−88	8
rt GL BA 19	0.160	3.71	0.001	14	−74	−12
lt GL BA 19	0.319	3.36	0.001	−10	−72	−8
lt Pcu BA 19	0.998	3.21	0.002	−6	−72	30
UPDR motor positive						
rt GPrC BA 4	<0.001	5.02	<0.001	12	−30	68
lt GPrC BA 4	0.257	4.09	<0.001	−10	−30	76
rt putamen	0.605	3.89	<0.001	26	−16	4

Abbreviations: lt = left; rt = right; GFm = middle frontal gyrus; GC = cingulate gyrus; GTm = middle temporal gyrus; LPi = inferior parietal lobe; GTi = inferior temporal gyrus; Gob = orbital gyrus; Cu = cuneus; Pcu = precuneus; GL = lingual gyrus; GPrC = precentral gyrus.

Tables 1 and 2 list the peaks of the most significant correlations with corrected *P* values of clusters with the height threshold set at $P < 0.005$.

Discussion

FDOPA PET, FDG PET, and multiple regression analysis were performed with the RCPM and UPDRS motor scores of a group of PD patients using SPM99 to identify the functional neuroanatomy of cognitive and motor impairment in PD. The correlation coefficient of the RCPM and UPRDS motor scores was close to zero, which allows us to separate motor and cognitive effects.

Correlations with cognitive function

The RCPM score was significantly positively correlated with the FDOPA Ki value in the left hippocampus and with rrCMRglc in the left dorsolateral prefrontal cortex (BA 9/46) and right retrosplenial cortex extending to the adjacent posterior cingulate cortex (BA 29/30/23) (Fig. 1). These three areas are strongly interconnected via the entorhinal cortex and the parahippocampal gyrus (Goldman-Rakic et al., 1984; Kobayashi and Amaral, 2003; Morris et al., 1999; Suzuki and Amaral, 1994; Van Hoesen, 1982) and were implicated in a previous PET study of Raven's Progressive Matrices (RPM) task in healthy young subjects (Esposito et al., 1999).

The main function of the hippocampus is long-term declarative memory (Gloor, 1997; Lepage et al., 1998; Mishkin et al., 1997), and the dorsolateral prefrontal cortex is implicated in working memory and memory retrieval and encoding (Cabeza and Nyberg, 2000; Fletcher and Henson, 2001) and executive cognitive function (D'Esposito et al., 1995; MacDonald et al., 2000). The retrosplenial cortex appears to be involved in spatial information processing and memory (Bottini et al., 1990; Maguire, 2001; McDonald et al.,

2001; Shallice et al., 1994; Valenstein et al., 1987) and can be considered to act as an interface between the working memory functions in the prefrontal areas and the long-term memory encoding in the medial temporal lobe (Kobayashi and Amaral, 2003). The implication of these three regions in our study supports the suggestion that the RCPM involves working memory and visuospatial processing as well as more long-term mnemonic processes (Mattay et al., 1996).

These three areas (prefrontal, retrosplenial, and medial temporal) have been implicated as part of a cognitive network involved in visual memory. Della-Maggiore et al. (2000) used PET activation with a delayed visual discrimination task that shares cognitive features with the RCPM and an analysis technique called seed-voxel partial least squares. They showed that in young subjects, the neutral network involved in this task included the prefrontal cortex (BA 10), fusiform gyrus, parahippocampal gyrus, posterior cingulate (precuneus), and inferior parietal gyrus. On the contrary, in the older subjects, the network included more anterior areas, that is, the caudate nucleus, the dorsolateral prefrontal cortex (BA 9/46), and the anterior cingulate gyrus (BA 32). The reliance on a frontostriatal network in older subjects could explain why prefrontal rrCMRglc correlated with RCPM performance in our PD patients. Moreover, Esposito et al. (1999) found an age-related increase of activity in the prefrontal and retrosplenial cortices in their PET study of the RPM task, suggesting that the retrosplenial cortex may also be included in the frontostriatal network for performance of the RCPM task. Indeed, we also observed a significant correlation between retrosplenial rrCMRglc and RCPM performance in our PD patients.

As stated earlier, the caudate nucleus is included in the older subjects' network in the study of Della-Maggiore et al. (2000). In PD patients, impairment of the nigrostriatal dopaminergic projection will likely disrupt this network. We initially speculated that in PD, the impairment of dopaminergic projection to the caudate nucleus would be the main cause of cognitive dysfunction; however, there was no correlation between the RCPM score and the FDOPA Ki value in the caudate nucleus. This negative finding may not indicate that the caudate nucleus is not important for the RCPM task, but that in PD patients, because of the impairment of nigrostriatal dopaminergic projection, there is compensatory recruitment of the alternate network, which includes the hippocampus. Indeed, the FDOPA Ki value in the left hippocampus was positively correlated with the RCPM scores. In addition, a previous PET activation study lends support to this notion: Dagher et al. (2001) reported increased hippocampal activation during the Tower of London task in PD patients compared to normal volunteers. In that study, the PD patients also showed deficient caudate activation during this task, perhaps indicating that the hippocampal activation represented recruitment of an alternate network to compensate for caudate dysfunction.

A role for mesolimbic dopamine projections to the hippocampus in cognitive function in PD is supported by the following evidence: Hippocampal dopamine D_2 receptor function has an influence on spatial working memory in animals (Umegaki et al., 2001; Wilkerson and Levin, 1999); there is a positive correlation between binding potential of [11C]FLB457, a D_2/D_3 receptor antagonist in the hippocampus, and memory function in a PET study of patients with Alzheimer's disease (Kemppainen et al., 2003).

A recent single photon emission tomography study indicated that the RCPM score was positively correlated with posterior parietal blood flow in PD patients on medication (Abe et al., 2003). The posterior parietal area has strong neural connections with the retrosplenial cortex and the prefrontal cortex (Cavada and Goldman-Rakic, 1989a,b; Kobayashi and Amaral, 2003; Van Hoesen, 1982) and has an important role in visuospatial working memory (Cabeza and Nyberg, 2000). Furthermore, this area was activated in a previous PET study of RPM task in young subjects (Esposito et al., 1999) and was included in the hippocampal network of the "young" (Della-Maggiore et al., 2000). Thus, this observation also indicates that for solving the RCPM, the posterior parietal–hippocampal network plays an important role in PD. It is notable that previous studies have shown a relationship between parietal hypometabolism in PD and cognitive dysfunction (Karbe et al., 1992; Kuhl et al., 1984; Mentis et al., 2002; Peppard et al., 1992; Piert et al., 1996; Wu et al., 2000).

Correlations with motor function

The UPDRS motor score, which increases with disability, was significantly inversely correlated with the FDOPA Ki value in the bilateral striatum (Fig. 2). This result is consistent with the assumption that impaired activity of the nigrostriatal dopaminergic system is the major cause of motor symptoms in PD. Although, the peaks were located in the putamen, the right caudate nucleus was also included in the correlated areas. This observation is consistent with previous reports (Brooks et al., 1990; Broussolle et al., 1999; Vingerhoets et al., 1997) and likely results from the occurrence of parallel loss of dopamine projections to putamen and caudate in PD.

Analysis of the FDG PET data showed a positive correlation between the UPDRS motor score and rrCMRglc in bilateral primary motor cortex and right caudal supplementary motor area (BA 6). The primary motor cortex and caudal SMA are involved in motor execution and belong to the CBGTC motor loop, which includes the putamen. Therefore, this finding is likely related to the dopaminergic deficit in the putamen. Evidence that primary motor hypermetabolism is related to motor deficits comes from two previous FDG PET studies that showed that levodopa infusion both improved UPDRS motor ratings and significantly decreased regional glucose metabolism in the primary motor cortex (Feigin et al., 2001, Hilker et al., 2002). The relative hypermetabolism in primary motor areas in PD may reflect a reduction in intracortical inhibition in the resting state, a hypothesis supported by certain neurophysiological studies. In a primate model of PD, neurons in the primary motor cortex discharge in long bursts synchronized across many cells that fail to elicit movement (Goldberg et al., 2002). Studies using transcranial magnetic stimulation showed that intracortical inhibition was markedly reduced in PD patients (Ridding et al., 1995; Strafella et al., 2000).

The UPDRS motor score was also significantly positively correlated with the rrCMRglc level in the right putamen. Previous FDG PET studies have shown a relative hypermetabolism in the putamen of PD patients compared to control volunteers (Antonini et al., 1995; Eidelberg et al., 1994; Mentis et al., 2002; Moeller and Eidelberg, 1997). Furthermore, a positive correlation between the relative hypermetabolism in the striatum and the impairment of motor function in PD patients has been observed (Eidelberg et al., 1994). This striatal hypermetabolism is probably the result of direct effects of dopamine deficiency on the striatum and complex feedback mechanisms, including up-regulation of D_2 receptors (Antonini et al., 1995).

The UPDRS motor score was significantly positively correlated with the FDOPA Ki value in the anterior cingulate gyrus (BA 24), consistent with the previous report of Rakshi et al. (1999). This

may reflect compensation of the relatively spared mesocortical projections in response to loss of mesostriatal dopamine. Recent PET activation and functional MRI (fMRI) studies have shown overactivation of the anterior cingulate in PD patients compared to controls with a variety of motor tasks (Catalan et al., 1999; Nakamura et al., 2001; Sabatini et al., 2000). These authors speculated that this overactivation might result from a recruitment mechanism aimed at compensating for the movement difficulties in patients with PD. It is conceivable that increased dopaminergic tone in the anterior cingulate, as demonstrated here, played a role in these alterations.

The UPDRS motor score was significantly inversely correlated with rrCMRglc in numerous cortical areas, including the primary and associative visual cortex, the occipitotemporal area, the orbitofrontal cortex, and the anterior cingulate gyrus bilaterally. While it is difficult to directly relate these effects to motor dysfunction per se, hypometabolism in primary visual as well as occipital, temporal, and frontal associative areas has been demonstrated previously in numerous imaging studies in PD (Arahata et al., 1999; Bohnen et al., 1999; Eberling et al., 1994; Hu et al., 2000; Imon et al., 1999). Bohnen et al. (1999) found a correlation between asymmetry in finger tapping and asymmetry in glucose metabolism in the primary visual cortex. In addition, occipital hypometabolism was observed in a primate model of PD (Schwartzman et al., 1988). Finally, Eidelberg et al. (1994), in a series of FDG PET studies, have described a PD-related metabolic pattern that involves cortical hypometabolism in prefrontal and parietooccipital areas (Carbon and Eidelberg, 2002). Moreover, the expression of this pattern correlates with numerous markers of striatal dopamine deficiency and motor dysfunction in PD patients, suggesting that it is directly related to loss of striatal dopamine.

The areas of inverse correlation between rrCMRglc and UPDRS motor scores are not necessarily involved in causing the motor dysfunction itself but may represent an effect of dopaminergic deficits in the striatum. For example, the corticostriatal projections from the occipitotemporal area, where the strongest inverse correlation of rrCMR with the UPDRS motor score was observed, terminate in the tail and genu of the caudate nucleus (Saint-Cyr et al., 1990; Yeterian and Pandya, 1995), which is thought to be involved in visual processing. Together, the occipitotemporal cortex and tail of the caudate form the "temporal association cortex loop" (Middleton and Strick, 1996; Rolls, 1999). Dysfunction in this loop would be more likely to account for deficits on visuospatial or visuomotor processes (Middleton and Strick, 1996; Mishkin and Appenzeller, 1987; Yeterian and Pandya, 1995). However, parietal and occipitotemporal rrCMRglc exhibited a significant correlation with motor UPDRS score but not with the RCPM score. We may therefore speculate that other factors, for example, related to the hippocampal network or to an executive motor system including the anterior cingulate gyrus might account for decreased RCPM performance in PD. This assumption may also explain why frontal hypometabolism does not always correlate with cognitive or motor dysfunction in PD (Bohnen et al., 1999; Carbon and Marie, 2003).

Conclusion

The FDOPA Ki value in the striatum was inversely, and the rrCMRglc level in the motor areas was positively, correlated with the UPDRS motor score. These regions belong to a motor CBGTC loop. Meanwhile, the FDOPA Ki value in the left hippocampus and the rrCMRglc level in the left middle frontal gyrus and the right retrosplenial cortex were positively correlated with the RCPM score, and these regions belong to a cognitive frontoparietal–hippocampal network. The UPDRS motor score was significantly positively correlated with FDOPA Ki value in the anterior cingulate gyrus, and we speculate that this finding may be related to up-regulation of dopamine synthesis in surviving dopamine neurons. The UPDRS motor score was significantly inversely correlated with rrCMRglc throughout the cortices including association areas and primary visual cortex, and we speculate that this may not directly cause motor dysfunction itself but represent an indirect effect of dopaminergic deficits in the striatum.

Acknowledgments

The abstract form of this report was shown in *Journal of Nuclear Medicine*; 43(Suppl): 244 pp., 2002. The authors thank Dr. Dale Bailey, MRC Cyclotron Unit, Hammersmith Hospital, for allowing us to use the software, 'kronos.' This study was supported by funds for Research on Longevity Science and for Comprehensive Research of Aging and Health from the Ministry and Welfare of Japan.

References

Aarsland, D., Tandberg, E., Larsen, J.P., Cummings, J.L., 1996. Frequency of dementia in Parkinson disease. Arch. Neurol. 53, 538–542.

Abe, Y., Kachi, T., Kato, T., Arahata, Y., Yamada, T., Washimi, Y., Iwai, K., Ito, K., Yanagisawa, N., Sobue, G., 2003. Occipital hypoperfusion in Parkinson's disease without dementia: correlation to impaired cortical visual processing. J. Neurol. Neurosurg. Psychiatry 74, 419–422.

Alexander, G.E., DeLong, M.R., Strick, P.L., 1986. Parallel organization of functionally segregated circuits linking basal ganglia and cortex. Annu. Rev. Neurosci. 9, 357–381.

Antonini, A., Vontobel, P., Psylla, M., Gunther, I., Maguire, P.R., Missimer, J., Leenders, K.L., 1995. Complementary positron emission tomographic studies of the striatal dopaminergic system in Parkinson's disease. Arch. Neurol. 52, 1183–1190.

Arahata, Y., Hirayama, M., Ieda, T., Koike, Y., Kato, T., Tadokoro, M., Ikeda, M., Ito, K., Sobue, G., 1999. Parieto-occipital glucose hypometabolism in Parkinson's disease with autonomic failure. J. Neurol. Sci. 163, 119–126.

Bohnen, N.I., Minoshima, S., Giordani, B., Frey, K.A., Kuhl, D.E., 1999. Motor correlates of occipital glucose hypometabolism in Parkinson's disease without dementia. Neurology 52, 541–546.

Bottini, G., Cappa, S., Geminiani, G., Sterzi, R., 1990. Topographic disorientation—A case report. Neuropsychologia 28, 309–312.

Brooks, D.J., Ibanez, V., Sawle, G.V., Quinn, N., Lees, A.J., Mathias, C.J., Bannister, R., Marsden, C.D., Frackowiak, R.S., 1990. Differing patterns of striatal 18F-Dopa uptake in Parkinson's disease, multiple system atrophy, and progressive supranuclear palsy. Ann. Neurol. 28, 547–555.

Broussolle, E., Dentresangle, C., Landais, P., Garcia-Larrea, L., Pollak, P., Croisile, B., Hibert, O., Bonnefoi, F., Galy, G., Froment, J.C., Comar, D., 1999. The relation of putamen and caudate nucleus 18F-Dopa uptake to motor and cognitive performances in Parkinson's disease. J. Neurol. Sci. 166, 141–151.

Cabeza, R., Nyberg, L., 2000. Imaging cognition II: an empirical review of 275 PET and fMRI studies. J. Cogn. Neurosci. 12, 1–47.

Calne, D.B., Snow, B.J., Lee, C., 1992. Criteria for diagnosing Parkinson's disease. Ann. Neurol. 32, S125–127 (Suppl.).

Carbon, M., Eidelberg, D., 2002. Modulation of regional brain function by

deep brain stimulation: studies with positron emission tomography. Curr. Opin. Neurol. 15, 451–455.
Carbon, M., Marie, R.M., 2003. Functional imaging of cognition in Parkinson's disease. Curr. Opin. Neurol. 16, 475–480.
Catalan, M.J., Ishii, K., Honda, M., Samii, A., Hallett, M., 1999. A PET study of sequential finger movement of varying length in patients with Parkinson's disease. Brain 122, 483–495.
Cavada, C., Goldman-Rakic, P.S., 1989a. Posterior parietal cortex in rhesus monkey: I. Parcellation of areas based on distinctive limbic and sensory corticocortical connections. J. Comp. Neurol. 287, 393–421.
Cavada, C., Goldman-Rakic, P.S., 1989b. Posterior parietal cortex in rhesus monkey: II. Evidence for segregated corticocortical networks linking sensory and limbic areas with the frontal lobe. J. Comp. Neurol. 287, 422–445.
Cronin-Golomb, A., Braun, A.E., 1997. Visuospatial dysfunction and problem solving in Parkinson's disease. Neuropsychology 11, 44–52.
Dagher, A., Owen, A.M., Boecker, H., et al., 2001. The role of the striatum and hippocampus in planning: a PET activation study in Parkinson's disease. Brain 124, 1020–1032.
D'Esposito, M., Detre, J.A., Alsop, D., Shin, R.K., Atlas, S., Grossman, M., 1995. The neural basis of the central executive system of working memory. Nature 378, 279–281.
Della-Maggiore, V., Sekuler, A.B., Grady, C.L., Bennett, P.J., Sekuler, R., McIntosh, A.R., 2000. Corticolimbic interactions associated with performance on a short-term memory task are modified by age. J. Neurosci. 20, 8410–8416.
Dubois, B., Pillon, B., 1997. Cognitive deficits in Parkinson's disease. J. Neurol. 244, 2–8.
Eberling, J.L., Richardson, B.C., Reed, B.R., Wolfe, N., Jagust, W.J., 1994. Cortical glucose metabolism in Parkinson's disease without dementia. Neurobiol. Aging 15, 329–335.
Eidelberg, D., Moeller, J.R., Dhawan, V., 1994. The metabolic topography of parkinsonism. J. Cereb. Blood Flow Metab. 14, 783–801.
Esposito, G., Kirkby, B.S., Van Horn, J.D., Ellmore, T.M., Berman, K.F., 1999. Context-dependent, neural system-specific neurophysiological concomitants of ageing: mapping PET correlates during cognitive activation. Brain 122, 963–979.
Farina, E., Gattellaro, G., Pomati, S., Magni, E., Perretti, A., Cannata, A.P., Nichelli, P., Mariani, C., 2000. Researching a differential impairment of frontal functions and explicit memory in early Parkinson's disease. Eur. J. Neurol. 7, 259–267.
Feigin, A., Fukuda, M., Dhawan, V., Przedborski, S., Jackson-Lewis, V., Mentis, M.J., Moeller, J.R., Eidelberg, D., 2001. Metabolic correlates of levodopa response in Parkinson's disease. Neurology 57, 2083–2088.
Folstein, M.F., Folstein, S.E., McHugh, P.R., 1975. "Mini-mental state". A practical method for grading the cognitive state of patients for the clinician. J. Psychiatr. Res. 2, 189–198.
Fletcher, P.C., Henson, R.N.A., 2001. Frontal lobes and human memory insights from functional neuroimaging. Brain 124, 849–881.
Friston, K.J., Holmes, A.P., Worsley, K.J., Poline, J.P., Frith, C.D., Frackowiak, R.S.J., 1995. Statistical parametric maps in functional imaging: a general linear approach. Hum. Brain Mapp. 2, 189–210.
Garnett, E.S., Firnau, G., Nahmias, C., 1983. Dopamine visualized in the basal ganglia of living man. Nature 305, 137–138.
Garnett, E.S., Nahmias, C., Firnau, G., 1984. Central dopaminergic pathways in hemiparkinsonism examined by positron emission tomography. Can. J. Neurol. Sci. 11 (Suppl. 1), 174–179.
Giladi, N., Treves, T.A., Paleacu, D., Shabtai, H., Orlov, Y., Kandinov, B., Simon, E.S., Korczyn, A.D., 2000. Risk factors for dementia, depression and psychosis in long-standing Parkinson's disease. J. Neural Transm. 107, 59–71.
Gloor, P., 1997. Function of Hippocampal System: Temporal Lobe and Limbic System. Oxford Univ. Press, New York, pp. 527–589.
Goldberg, J.A., Boraud, T., Maraton, S., Haber, S.N., Vaadia, E., Bergman, H., 2002. Enhanced synchrony among primary motor cortex neurons in the 1-methyl-4-phenyl-1,2,3,6-tetrahydropyridine primate model of Parkinson's disease. J. Neurosci. 22, 4639–4653.
Goldman-Rakic, P.S., Selemon, L.D., Schwartz, M.L., 1984. Dual pathways connecting the dorsolateral prefrontal cortex with the hippocampal formation and parahippocampal cortex in the rhesus monkey. Neuroscience 12, 719–743.
Hilker, R., Voges, J., Thiel, A., Ghaemi, M., Herholz, K., Sturm, V., Heiss, W.D., 2002. Deep brain stimulation of the subthalamic nucleus versus levodopa challenge in Parkinson's disease: measuring the on- and off-conditions with FDG-PET. J. Neural Transm. 109, 1257–1264.
Hoehn, M.M., Yahr, M.D., 1967. Parkinsonism: onset, progression and mortality. Neurology 17, 427–442.
Holthoff, V.A., Vieregge, P., Kessler, J., Pietrzyk, U., Herholz, K., Bonner, J., Wagner, R., Wienhard, K., Pawlik, G., Heiss, W.D., 1994. Discordant twins with Parkinson's disease: positron emission tomography and early signs of impaired cognitive circuits. Ann. Neurol. 36, 176–182.
Holthoff-Detto, V.A., Kessler, J., Herholz, K., Bonner, H., Pietrzyk, U., Wurker, M., Ghaemi, M., Wienhard, K., Wagner, R., Heiss, W.D., 1997. Functional effects of striatal dysfunction in Parkinson disease. Arch. Neurol. 54, 145–150.
Hu, M.T., Taylor-Robinson, S.D., Chaudhuri, K.R., Bell, J.D., Labbe, C., Cunningham, V.J., Koepp, M.J., Hammers, A., Morris, R.G., Turjanski, N., Brooks, D.J., 2000. Cortical dysfunction in non-demented Parkinson's disease patients: a combined (31)P-MRS and (18)FDG-PET study. Brain 123, 340–352.
Hutchins, G.D., Holden, J.E., Koeppe, R.A., Halama, J.R., Gatley, S.J., Nickles, R.J., 1984. Alternative approach to single-scan estimation of cerebral glucose metabolic rate using glucose analogs, with particular application to ischemia. J. Cereb. Blood Flow Metab. 4, 35–40.
Imon, Y., Matsuda, H., Ogawa, M., Kogure, D., Sunohara, N., 1999. SPECT image analysis using statistical parametric mapping in patients with Parkinson's disease. J. Nucl. Med. 40, 1583–1589.
Ito, K., Nagano-Saito, A., Kato, T., Arahata, Y., Nakamura, A., Kawasumi, Y., Hatano, K., Abe, Y., Yamada, T., Kachi, T., Brooks, D.J., 2002. Striatal and extrastriatal dysfunction in Parkinson's disease with dementia. A 6-[^{18}F]fluoro-L-dopa PET study. Brain 125, 1358–1365.
Janvin, C., Aarsland, D., Larsen, J.P., Hugdahl, K., 2003. Neuropsychological profile of patients with Parkinson's disease without dementia. Dement. Geriatr. Cogn. Disord. 15, 126–131.
Karbe, H., Holthoff, V., Huber, M., Herholz, K., Wienhard, K., Wagner, R., Heiss, W.D., 1992. Positron emission tomography in degenerative disorders of the dopaminergic system. J. Neural Transm., Parkinson's Dis. Dement. Sect. 4, 121–130.
Kemppainen, N., Laine, M., Laakso, M.P., Kaasinen, V., Nagren, K., Vahlberg, T., Kurki, T., Rinne, J.O., 2003. Hippocampal dopamine D_2 receptors correlate with memory functions in Alzheimer's disease. Eur. J. Neurosci. 18, 149–154.
Kobayashi, Y., Amaral, D.G., 2003. Macaque monkey retrosplenial cortex: II. Cortical afferents. J. Comp. Neurol. 466, 48–79.
Kretshmann, H.J., Weinirich, W., 1992. Neurotransmitters and Neuromodulators: Cranial Neuroimaging and Clinical Neuroanatomy. Thieme, New York, pp. 343–349.
Kuhl, D.E., Metter, E.J., Riege, W.H., 1984. Patterns of local cerebral glucose utilization determined in Parkinson's disease by the [18F]fluorodeoxyglucose method. Ann. Neurol. 15, 419–424.
Leenders, K.L., Salmon, E.P., Tyrrell, P., Perani, D., Brooks, D.J., Sager, H., Jones, T., Marsden, C.D., Frackowiak, R.S., 1990. The nigrostriatal dopaminergic system assessed in vivo by positron emission tomography in healthy volunteer subjects and patients with Parkinson's disease. Arch. Neurol. 47, 1290–1298.
Lepage, M., Habib, R., Tulving, E., 1998. Hippocampal PET activations of memory encoding and retrieval: the HIPER model. Hippocampus 8, 313–322.
MacDonald, A.W., Cohen, J.D., Stenger, V.A., et al., 2000. Dissociating the role of the dorsolateral prefrontal and anterior cingulate cortex in cognitive control. Science 288, 1835–1838.
Maguire, E.A., 2001. The retrosplenial contribution to human navigation: a review of lesion and neuroimaging findings. Scand. J. Psychol. 42, 225–238.

Martin, W.R., Palmer, M.R., Patlak, C.S., Calne, D.B., 1989. Nigrostriatal function in humans studied with positron emission tomography. Ann. Neurol. 26, 535–542.

Mattay, V.S., Berman, K.F., Ostrem, J.L., Esposito, G., Van Horn, J.D., Bigelow, L.B., Weinberger, D.R., 1996. Dextroamphetamine enhances "neural network-specific" physiological signals: a positron-emission tomography rCBF study. J. Neurosci. 16, 4816–4822.

Mazziotta, J.C., Toga, A.W., Evans, A., Fox, P., Lancaster, J., 1995. A probabilistic atlas of the human brain: theory and rationale for its development. The International Consortium for Brain Mapping (ICBM). NeuroImage 2, 89–101.

McDonald, C.R., Crosson, B., Valenstein, E., Bowers, D., 2001. Verbal encoding deficits in a patient with a left retrosplenial lesion. Neurocase 7, 407–417.

McKeith, I.G., Galasko, D., Kosaka, K., Perry, E.K., Dickson, D.W., Hansen, L.A., Salmon, D.P., et al., 1996. Consensus guidelines for the clinical and pathologic diagnosis of dementia with Lewy bodies (DLB): report of the consortium on DLB international workshop. Neurology 47, 1113–1124.

Mentis, M.J., McIntoshi, A.R., Perrine, K., Dhawan, V., Berlin, B., Feigin, A., Edwards, C., Mattis, P., Eidelberg, D., 2002. Relationships among the metabolic patterns that correlate with mnemonic, visuospatial, and mood symptoms in Parkinson's disease. Am. J. Psychiatry 159, 746–754.

Middleton, F.A., Strick, P.L., 1996. The temporal lobe is a target of output from the basal ganglia. Proc. Natl. Acad. Sci. U.S.A. 93, 8683–8687.

Mishkin, M., Appenzeller, T., 1987. The anatomy of memory. Sci. Am. 256, 80–89.

Mishkin, M., Suzuki, W.A., Gadian, D.G., Vargha-Khadem, F., 1997. Hierarchical organization of cognitive memory. Philos. Trans. R. Soc. Lond. B. Biol. Sci. 352, 1461–1467.

Moeller, J.R., Eidelberg, D., 1997. Divergent expression of regional metabolic topographies in Parkinson's disease and normal ageing. Brain 120, 2197–2206.

Morris, R., Pandya, D.N., Petrides, M., 1999. Fiber system linking the middorsolateral frontal cortex with the retrosplenial/presubicular region in the rhesus monkey. J. Comp. Neurol. 407, 183–192.

Nagano, A.S., Ito, K., Kato, T., Arahata, Y., Kachi, T., Hatano, K., Kawasumi, Y., Nakamura, A., Yamada, T., Abe, Y., Ishigaki, T., 2000. Extrastriatal mean regional uptake of Fluorine-18-FDOPA in the normal aged brain—An approach using MRI-aided spatial normalization. NeuroImage 11, 760–766.

Nahmias, C., Garnett, E.S., Firnau, G., Lang, A., 1985. Striatal dopamine distribution in parkinsonian patients during life. J. Neurol. Sci. 69, 223–230.

Nakamura, T., Ghilardi, M.F., Mentis, M., Dhawan, V., Fukuda, M., Hacking, A., Moeller, J.R., Ghez, C., Eidelberg, D., 2001. Functional networks in motor sequence learning: abnormal topographies in Parkinson's disease. Hum. Brain Mapp. 12, 42–60.

Parent, A., Hazrati, L.N., 1995. Functional anatomy of the basal ganglia: I. The cortico-basal ganglia-thalamo-cortical loop. Brain. Res. Brain Res. Rev. 20, 91–127.

Patlak, C.S., Blasberg, R.G., 1985. Graphical evaluation of blood-to-brain transfer constants from multiple-time uptake data. Generalizations. J. Cereb. Blood Flow Metab. 5, 584–590.

Peppard, R.F., Martin, W.R., Carr, G.D., Grochowski, E., Schulzer, M., Guttman, M., McGeer, P.L., Phillips, A.G., Tsui, J.K., Calne, D.B., 1992. Cerebral glucose metabolism in Parkinson's disease with and without dementia. Arch. Neurol. 49, 1262–1268.

Phelps, M.E., Huang, S.C., Hoffman, E.J., Selin, C., Sokoloff, L., Kuhl, D.E., 1979. Tomographic measurement of local cerebral glucose metabolic rate in humans with (F-18)2-fluoro-2-deoxy-D-glucose: validation of method. Ann. Neurol. 6, 371–388.

Piert, M., Koeppe, R.A., Giordani, B., Minoshima, S., Kuhl, D.E., 1996. Determination of regional rate constants from dynamic FDG-PET studies in Parkinson's disease. J. Nucl. Med. 37, 1115–1122.

Rakshi, J.S., Uema, T., Ito, K., Bailey, D.L., Morrish, P.K., Ashburner, J., Dagher, A., Jenkins, I.H., Friston, K.J., Brooks, D.J., 1999. Frontal, midbrain and striatal dopaminergic function in early and advanced Parkinson's disease: a 3D [18F]dopa-PET study. Brain 122, 1637–1650.

Raven, J.C., 1962. Standard Progressive Matrices: Set A, A_B, B Lewis, London.

Ridding, M.C., Inzelberg, R., Rothwell, J.C., 1995. Changes in excitability of motor cortical circuitry in patients with Parkinson's disease. Ann. Neurol. 37, 181–188.

Rinne, J.O., Portin, R., Ruottinen, H., Nurmi, E., Bergman, J., Haaparanta, M., Solin, O., 2000. Cognitive impairment and the brain dopaminergic system in Parkinson disease: [18F]fluorodopa positron emission tomographic study. Arch. Neurol. 57, 470–475.

Rolls, E.T., 1999. Pharmacology and Neurochemistry of Reward, and Neural Output Systems for Reward: The Brain and Emotion. Oxford, New York, pp. 168–204.

Sabatini, U., Boulanouar, K., Fabre, N., Martin, F., Carel, C., Colonnese, C., Bozzao, L., Berry, I., Montastruc, J.L., Chollet, F., Rascol, O., 2000. Cortical motor reorganization in akinetic patients with Parkinson's disease: a functional MRI study. Brain 123, 394–403.

Saint-Cyr, J.A., Ungerleider, L.G., Desimone, R., 1990. Organization of visual cortical inputs to the striatum and subsequent outputs to the pallido-nigral complex in the monkey. J. Comp. Neurol. 298, 129–156.

Schwartzman, R.J., Alexander, G.M., Ferraro, T.N., Grothusen, J.R., Stahl, S.M., 1988. Cerebral metabolism of parkinsonian primates 21 days after MPTP. Exp. Neurol. 102, 307–313.

Shallice, T., Fletcher, P., Frith, C.D., Grasby, P., Frackowiak, R.S., Dolan, R.J., 1994. Brain regions associated with acquisition and retrieval of verbal episodic memory. Nature 368, 633–635.

Strafella, A.P., Valzania, F., Nassetti, S.A., Tropeani, A., Bisulli, A., Santangelo, M., Tassinari, C.A., 2000. Effects of chronic levodopa and pergolide treatment on cortical excitability in patients with Parkinson's disease: a transcranial magnetic stimulation study. Clin. Neurophysiol. 111, 1198–1202.

Sugishita, M., Yamasaki, K., 1993. Japanse Rafen's Coloured Progressive Matrices. Nihon Bunka Kagakusha, Tokyo.

Suzuki, W.A., Amaral, D.G., 1994. Perirhinal and parahippocampal cortices of the macaque monkey: cortical afferents. J. Comp. Neurol. 350, 497–533.

Umegaki, H., Munoz, J., Meyer, R.C., Spangler, E.L., Yoshimura, J., Ikari, H., Iguchi, A., Ingram, D.K., 2001. Involvement of dopamine D(2) receptors in complex maze learning and acetylcholine release in ventral hippocampus of rats. Neuroscience 103, 27–33.

Valenstein, E., Bowers, D., Verfaellie, M., Heilman, K.M., Day, A., Watson, R.T., 1987. Retrosplenial amnesia. Brain 110, 1631–1646.

Van Hoesen, G.W., 1982. The parahippocampal gyrus new observations regarding its cortical connection in the monkey. Trends Neurosci. 5, 345–350.

Vingerhoets, F.J., Schulzer, M., Calne, D.B., Snow, B.J., 1997. Which clinical sign of Parkinson's disease best reflects the nigrostriatal lesion? Ann. Neurol. 41, 58–64.

Wang, G.J., Volkow, N.D., Wolf, A.P., Brodie, J.D., Hitzemann, R.J., 1994. Intersubject variability of brain glucose metabolic measurements in young normal males. J. Nucl. Med. 35, 1457–1466.

Weder, B.J., Leenders, K.L., Vontobel, P., Nienhusmeier, M., Keel, A., Zaunbauer, W., Vonesch, T., Ludin, H.P., 1999. Impaired somatosensory discrimination of shape in Parkinson's disease: association with caudate nucleus dopaminergic function. Hum. Brain Mapp. 8, 1–12.

Wilkerson, A., Levin, E.D., 1999. Ventral hippocampal dopamine D_1 and D_2 systems and spatial working memory in rats. Neuroscience 89, 743–749.

Wu, J.C., Iacono, R., Ayman, M., Salmon, E., Lin, S.D., Carlson, J., Keator, D., Lee, A., Najafi, A., Fallon, J., 2000. Correlation of intellectual impairment in Parkinson's disease with FDG PET scan. NeuroReport 11, 2139–2144.

Yeterian, E.H., Pandya, D.N., 1995. Corticostriatal connections of extrastriate visual areas in rhesus monkeys. J. Comp. Neurol. 352, 436–457.

Movement Disorders
Vol. 19, No. 7, 2004, pp. 801–806

Visual Hallucination in Parkinson's Disease With FDG PET

Atsuko Nagano-Saito, MD, PhD,[1,2]* Yukihiko Washimi, MD, PhD,[2] Yutaka Arahata, MD, PhD,[1,2] Katsushige Iwai, MD,[2] Shoji Kawatsu, MD, PhD,[1] Kengo Ito, MD, PhD,[1] Akinori Nakamura, MD, PhD,[1] Yuji Abe, MD, PhD,[2] Takako Yamada, MD, PhD,[2] Takashi Kato, MD, PhD,[1] and Teruhiko Kachi, MD, PhD[2]

[1]*Department of Brain Science and Molecular Imaging, National Institute for Longevity Sciences, National Center for Geriatrics and Gerontology, Obu, Japan*
[2]*Department of Neurology, Chubu National Hospital, Obu, Japan*

Abstract: To determine the characteristics of cerebral glucose metabolism in Parkinson's disease patients with visual hallucinations, group comparison studies using [^{18}F]fluorodeoxyglucose positron emission tomography were performed. Nondemented Parkinson's disease patients in advanced stages were classified into two groups: (1) patients without visual hallucinations; (2) patients with visual hallucinations. Compared to patients without hallucinations, the relative regional cerebral glucose metabolic rate was greater in the frontal areas in patients with visual hallucinations, and the increase reached a significant level in the left superior frontal gyrus. Relative frontal hypermetabolism may be a feature of Parkinson's disease patients with visual hallucinations.
© 2004 Movement Disorder Society

Key words: Parkinson's disease; visual hallucination; [^{18}F]fluorodeoxyglucose; FDG; positron emission tomography (PET)

Visual hallucinations are not uncommon among patients with Parkinson's disease (PD), especially at an advanced stage,[1] and are strongly associated with cognitive impairment.[2–6] To our knowledge, there was only one single photon emission computed tomography (SPECT) study concerning visual hallucination in PD,[7] and no positron emission tomography (PET) studies have been reported yet. According to the SPECT report, patients with hallucinations showed significantly lower cerebral blood flow in left temporal and upper temporo-occipital regions than patients without hallucinations. However, region of interest analysis was used, and the whole brain was not evaluated in this report.

Statistical parametric mapping (SPM) was developed by Friston and colleagues[8] for analysis of functional imaging studies of the human brain. Included in SPM are a program that spatially transforms images into standard stereotactic space and a statistical program that generates statistical parametric maps by applying different statistical tests on a voxel-by-voxel basis. To locate the regional abnormalities in relative regional cerebral glucose metabolic rate (rrCMRglc) related to visual hallucinations, group comparisons of the rrCMRglc between two PD groups were performed using SPM99.

PATIENTS AND METHODS

Patients

Eight nondemented patients with PD and repeated visual hallucinations were recruited in this study. All visual hallucinations that patients reported were of human beings. All patients fulfilled UK Brain Bank criteria[9] for the diagnosis of PD. Detailed interview with patients and their families confirmed that they had neither delirium nor memory deficits. Patients who fulfilled the Consortium on Dementia with Lewy bodies (DLB) International Workshop criteria[10] or whose Mini-Mental State Examination (MMSE)[11] scores were less than 26 were excluded. The lag between the onset of parkinsonism and visual hallucinations was at least 2 years, and visual hallucinations persisted even after drug reductions. This group was referred to as VH (7 patients with predominantly left PD signs and 1 with predominantly right PD signs). There were 11 age-, Hoehn and Yahr

*Correspondence to: Dr. Atsuko Nagano-Saito, Department of Brain Science and Molecular Imaging, National Institute for Longevity Sciences, National Center for Geriatrics and Gerontology, 36-3 Gengo Morioka-Cho, Obu, Aichi 474-8522, Japan. E-mail: anagano@sannet.ne.jp
Received 22 November 2002; Revised 16 January 2004; Accepted 12 February 2004
Published online 21 April 2004 in Wiley InterScience (www.interscience.wiley.com). DOI: 10.1002/mds.20129

TABLE 1. *Clinical features of patients*

	N-VH (n = 11)	VH (n = 8)	*P*
Age (yr)	66.0 ± 7.5	67.6 ± 6.2	0.622
Duration of disease (yr)	5.1 ± 3.8	8.6 ± 5.0	0.071
Hoehn and Yahr scale	3.2 ± 0.5	3.6 ± 0.9	0.353
MMSE score	28.5 ± 1.7	28.3 ± 1.8	0.801
UPDRS Motor score	43.1 ± 15.5	39.2 ± 10.3[a]	0.589
Tremor score	5.5 ± 4.4	2.2 ± 4.0[a]	0.140
Rigidity score	10.0 ± 3.7	8.3 ± 5.6[a]	0.469

[a]n = 6.

P values of simple *t* test between two groups are listed in the rightmost column. N-VH, no visual hallucinations; VH, visual hallucinations; MMSE, Mini-Mental State Examination; UPDRS, Unified Parkinson's Disease Rating Scale.

scale-,[12] and MMSE score-matched PD patients, without visual hallucinations were recruited (N-VH group, 5 patients with predominantly left PD signs and 6 with predominantly right PD signs). Each group had 2 patients with motor fluctuations, and no patient had dyskinesia.

Age, duration of disease, Hoehn and Yahr scale, MMSE score, and Unified Parkinson's Disease Rating Scale (UPDRS) Motor score obtained with the patients in the *off* state are shown in Table 1. Simple *t* test indicated no differences between two groups. Patients' anti-PD medications and results of χ^2 distribution (for number of medicated patients) and simple *t* test (for dosage of medication) between two groups are shown in Table 2. Four types of dopamine agonists were used, and the dosages were calculated in terms of bromocriptine with the following formula: bromocriptine 10 mg = pergolide 550 μg = cabergoline 2 mg = talipexol 1.6 mg.[13] One VH patient was occasionally medicated with dopamine blocker, and none of other patients were receiving treatment for the hallucinations. Each patient was assessed clinically by a neurologist before their PET study and at least 24 hours after discontinuing their PD medications in the *off* state. Motor status of patients during the PET scans was almost the same as when UPDRS Motor scores were obtained, and no patients complained of visual hallucinations during the scans.

In addition, a control group of 13 aged-matched healthy volunteers (mean age ± SD, 66.2 ± 4.9 years; mean MMSE score ± SD, 29.1 ± 1.0) were studied. Permission to perform these studies was obtained from the Ethics Committee of Chubu National Hospital.

Data Acquisition and Analysis

[^{18}F]Fluorodeoxyglucose PET.

Subjects fasted for at least 4 hours before scans. [^{18}F]Fluorodeoxyglucose (FDG)-PET studies were performed using an ECAT EXACT HR47 (CTI/Siemens, Knoxville, TN) in two-dimensional acquisition mode, which yielded 47 simultaneous planes, with an axial full-width half-maximum (FWHM) resolution of 4.1 mm and an in-plane resolution of 3.9 mm × 3.9 mm. Three hundred to 370 MBq of FDG was infused intravenously into each subject over 120 seconds. The protocol included 18 time frames (12 × 2 min, 4 × 4 min, 2 × 10 min) over 60 minutes, and a summed-up-image was obtained by summing the last three frames, consisting of data from 36 to 60 minutes after injection. A mold made of air cushion was fitted to minimize head movement. The subject was positioned in the scanner so that the entire brain was within the field of view. Attenuation of 511 keV annihilation radiation was measured with a 10-minute, two-dimensional transmission scan performed prior to tracer injection, using a retractable 68Ga/68Ge source.

Spatial and Global Normalization.

The FDG summed images were directly transformed into standard stereotaxic space using the PET template in

TABLE 2. *Medications of patients*

Medications	N-VH (n = 11)	VH (n = 8)	*P* value
Dopamine precursor	8	8	0.107
dosage of levodopa (mg/day)	255 ± 202 (350 ± 141)	322 ± 140 (388 ± 181)	0.157
Dopamine agonist[a]	2	4	0.141
dose of bromocriptine (mg/day)	2.5 ± 5.5 (13.6 ± 0)	5.2 ± 8.6 (10.3 ± 10.0)	0.405
Dopamine release accelerator	1	1	0.811
dose of amantadine (mg/day)	9.1 ± 30.1 (100 ± 0)	12.5 ± 35.5 (100 ± 0)	0.824
Anticholinergic drug	4	1	0.243
dose of trihexyphenidyl (mg/day)	1.8 ± 2.6 (5.0 ± 1.2)	0.5 ± 1.4 (4.0 ± 0)	0.213
Noradrenaline precursor	0	3	0.027
dose of droxidopa (mg/day)	0 ± 0 (0 ± 0)	225 ± 349 (600 ± 300)	0.045

[a]Four types of dopamine agonists were used, then the dosages were calculated in terms of bromocriptine.

The numbers of those receiving the drug and average dosages of whole group are listed. Average group dosages for those receiving the drug are also listed in the parentheses. *P* values of χ^2 distribution (for number of medicated patients) and simple *t* test (for dosage of medication) between two groups are listed in the rightmost column. N-VH, no visual hallucinations; VH, visual hallucinations.

SPM. After spatial normalization, the images were smoothed with an isotropic Gaussian kernel (FWHM = 10 mm) and, to eliminate the variation in mean glucose utilization and to better detect disease-specific change,[14,15] the voxel values of the smoothed images were globally normalized. The mean value of the voxels, whose counts were higher than 60% of the highest value, which included almost all of the cortex, thalamus, and striatum, was calculated for global normalization for each subject. Then, to get globally normalized images, the voxel values of the smoothed images were divided by the mean value. The values in the globally normalized images were considered to approximate rrCMRglc.[16]

Group Comparisons in PET With SPM

Group comparison between rrCMRglc images of normal volunteers and those of N-VH and VH was performed. Then, group comparison between the two PD groups was performed. All comparisons were carried out for each voxel using the general linear approach[8] using SPM99. The effect of each group difference was tested, and the result was indicated as a T map. The P values associated with regional differences in rrCMRglc were corrected for multiple dependent comparisons. The height threshold was set at $P < 0.01$ with extent threshold set at $P < 0.05$. In addition, peaks meeting a more liberal criterion of height threshold set at $P < 0.05$ with extent threshold set at $P < 0.05$ was also listed as reference. A mask made from the gray-matter component of the magnetic resonance imaging (MRI) template in SPM was used for these analyses, so that white matter was excluded.

Region of Interest Analysis

Region of interest (ROI) analysis was also performed. On each of the spatially and globally normalized rrCMRglc images of patients, common ROIs were drawn bilaterally for the dorsolateral prefrontal (dorsal parts of Brodmann area [BA] 6, 8, 9), primary visual (BA 17), occipital association (lateral parts of BA 18, 19), and primary motor (BA 4) cortex. The location of ROI was guided by the results of the SPM analysis mentioned above. The mean regional rrCMRglc values were calculated for each region; then, statistical analyses were performed by means of t testing for the two patients group for each region. In all cases, the significance level was set at $P < 0.01$.

RESULTS

SPM Analysis

Compared to normal volunteers, the rrCMRglc was lower in the occipital, occipitotemporal areas (BA 17,18,19,20,21,37), and parietal areas (BA 7,39,40) in both PD groups, and in frontal areas in N-VH patients. The decrease of rrCMRglc in the posterior areas was 24% greater in VH compared to N-VH. Compared to normal controls, the rrCMRglc was greater in the pons and the cerebellum in both of the PD groups. The cerebellar peaks seemed to correspond to dentate, vestibular, and other cerebellar nuclei. In addition, the rrCMRglc was greater in precentral and postcentral gyrus extending to middle frontal gyrus in VH compared to controls. Although the difference was not significant at the 0.01 threshold, the rrCMRglc of N-VH was also greater than controls in precentral gyrus with the height threshold of $P < 0.05$.

Compared to N-VH, the rrCMRglc in the left superior frontal gyrus was greater in VH (Fig. 1). There was no region where the rrCMRglc of VH was lower than that of N-HV. Although, the difference was not significant at the 0.01 threshold, the rrCMRglc in widespread frontal areas was greater in VH compared to N-VH with the height threshold of $P < 0.05$. Table 3 lists the peaks of the most significant differences in these results.

ROI Analysis

There was no significant difference of rrCMRglc between N-VH and VH, at the threshold of $P < 0.01$. However, rrCMRglc of both sides of dorsolateral prefrontal cortex tended to be higher in VH than that of N-VH, and this tendency was stronger in the left side (Table 4).

DISCUSSION

Clinical Features

Among clinical features and medication, only the dose of noradrenaline precursor was significantly different between N-VH and VH. However, so far, there have been no reports to support a relationship between noradrenaline precursor and visual hallucination. While the difference was not significant at the 0.05 threshold, duration of disease tended to be longer, and dopamine precursor and dopamine agonist dose tended to be greater in VH than N-VH. The tendency of longer duration of disease and greater amount of dopamine agonist is consistent with previous reports.[4,6] These nonsignificant differences might play a role in the existence of visual hallucination or the difference of rrCMRglc. Larger amounts of dopamine precursor or dopamine agonist might have been needed for VH patients, and this increase could have potentially increased rrCMRglc in the frontal cortex; however, confirmation with a greater number of patients is needed.

FIG. 1. Significantly different regions ($P < 0.01$, corrected) of relative regional cerebral metabolic rate for glucose (rrCMRglc) with group comparison study. Compared to patients with no visual hallucinations, an increase of rrCMRglc is observed in the left superior frontal gyrus in patients with visual hallucinations.

Normal Controls versus PD

The pattern of decreased and increased rrCMRglc in N-VH and VH, compared to normal controls, was similar, except for frontal areas. The decrease of rrCMRglc seen in both PD groups in the occipital and parietal areas is consistent with previous FDG studies.[17–20] The increase of rrCMRglc in cerebellum and precentral gyrus is consistent with previous reports, indicating that the glucose metabolism in these areas was preserved in nondemented PD patients.[18,19]

N-VH versus VH

The rrCMRglc tended to be greater in the frontal areas in VH compared to N-VH, and the increase reached a significant level in the left superior frontal gyrus. The

TABLE 3. *Peak coordinates in SPM analyses of rrCMRglc*

	Cluster level		Voxel level				
	P corrected	k	*x*	*y*	*z*	T	Regions
NC > N-VH	<0.001	9078	−4	−48	40	7.10	lt PCu/GC (BA 7/31)
			−20	−92	−6	5.64	lt GL (BA 18/17)
	<0.001	7575	44	32	34	6.49	rt GFm (BA 9)
			54	32	10	4.75	rt GFm((BA 46)
	<0.001	2702	56	−38	−10	5.34	rt GTi (BA 20/37)
			58	−32	6	3.50	rt GTm (BA 21)
	<0.001	3599	−52	−30	−6	4.90	lt GTm/GTi (BA 20/37)
			−54	−60	−26	4.01	lt GTi (BA 37)
NC > VH	<0.001	19072	−2	−88	−10	7.53	lt GL (BA 18/17)
			64	−22	34	6.39	rt LPi (BA 40)
NC < N-VH	0.002	1692	12	−56	−32	6.51	rt dentate nucleus
			10	−36	−32	4.99	rt vestibular nucleus
NC < VH	<0.001	2182	−24	−54	−42	5.30	lt dentate nucleus
			−10	−40	−32	3.67	lt vestibular nucleus
	0.001	1874	12	−12	60	5.27	rt GFs (BA 6/4)
			10	−40	68	4.40	rt GPoC (BA 3/1/2)
	0.001	1751	−14	−36	66	4.65	lt GPoC (BA 3/1/2)
			−24	−22	72	4.17	lt GPrC (BA6/4)
N-VH < VH	0.030	1113	−24	20	60	4.45	lt GFs (BA 6/8)
			−16	46	38	4.11	lt GFs (BA 8/9)

Maximum peak coordinate for each anatomical region is listed. Abbreviations: lt, left; rt, right; BA, Brodmann area; PCu, precuneus; GC, cingulate gyrus; GFs, superior frontal gyrus; GFm, middle frontal gyrus; GTm, middle temporal gyrus; GTi, inferior temporal gyrus; GL, lingual gyrus; LPi, inferior parietal lobe; GPoC, postcentral gyrus; GPrC, precentral gyrus; SPM, statistical parametric mapping; rr CMRglc; relative regional cerebral metabolic rate for glucose; N-VH, no visual hallucinations; VH, visual hallucinations.

TABLE 4. *Region of interest analyses of rrCMRglc*

	N-VH	VH	*P*
Dorsolateral prefrontal cortex			
lt	0.87 ± 0.03	0.93 ± 0.08	0.02
rt	0.87 ± 0.04	0.92 ± 0.08	0.07
Primary visual cortex			
lt	0.76 ± 0.06	0.76 ± 0.07	0.98
rt	0.75 ± 0.06	0.76 ± 0.07	0.91
Occipital association cortex			
lt	0.90 ± 0.07	0.89 ± 0.10	0.89
rt	0.88 ± 0.07	0.86 ± 0.08	0.68
Primary motor cortex			
lt	1.01 ± 0.08	1.02 ± 0.05	0.94
rt	1.02 ± 0.09	1.03 ± 0.04	0.79

P values of simple *t* test are listed in the rightmost column. rrCMRglc, relative regional cerebral metabolic rate for glucose; lt, left; rt, right; N-VH, no visual hallucinations; VH, visual hallucinations.

prefrontal regions, including BA 8/9 are implicated in working memory[21,22] and executive cognitive function.[23] In addition to this, primate studies indicated that the prefrontal cortex plays a role in exerting executive control of memory retrieval from the site of long-term storage.[24,25] The occipital and occipitotemporal areas are considered as visual areas.[26,27]

A previous ^{99m}Tc-labeled hexamethyl propyleneamine oxime SPECT study indicated that hallucinatory patients showed significantly lower semiquantitative cerebral blood flow in the left temporal and upper temporo-occipital regions than nonhallucinatory patients.[7] The discrepancy between their and our results might be attributed to three aspects as follows: (1) the difference between cerebral blood flow and glucose metabolism, (2) the difference between medication-induced visual hallucinations and visual hallucinations that persist even after drug reductions, or (3) if demented-patients were included or not.

A previous study of patients with ischemic infarction showed that positive spontaneous visual phenomena (PSVP) were observed in patients with relatively small lesions limited to posterior regions and that larger lesions destroying anteriorly located visual association areas precluded the development of PSVP.[28] A functional MRI study while subjects thought of missing last words of a sentence comparing normal subjects with schizophrenia patients showed that there were no significant group differences in regional brain responses. However, the correlation coefficients between left temporal cortex and left dorsolateral prefrontal cortex were significantly lower in the schizophrenic group and were negatively correlated with the severity of auditory hallucination.[29] Thus, imbalance of activity between primary sensory regions and anterior associative regions, including dorsolateral prefrontal cortex may play a part in PSVP or auditory hallucination. Another study concluded that visual pathway lesions impair visual input and may result in hallucinations from defective visual processing or an abnormal cortical release phenomenon.[30] Our finding may be consistent with this theory.

CONCLUSION

Using FDG PET, group comparison studies were performed to determine the specific regions of the brain that are related to visual hallucinations in PD patients. The pattern of relative hypermetabolism in the frontal cortex with relative hypometabolism in the posterior areas is likely a metabolic feature of visual hallucinations in PD patients. The mechanism of hallucination is unknown, and more studies need to be conducted.

Acknowledgments: We thank Dr. Alain Dagher, Montreal Neurological Institute, McGill University, for reading this report and providing thoughtful remarks. This study was supported by funds for Research on Longevity Science and for Comprehensive Research of Aging and Health from the Ministry and Welfare of Japan.

REFERENCES

1. Korczeyn AD. Hallucinations in Parkinson's disease. Lancet 2001; 358:1031–1032.
2. Barnes J, David S. Visual hallucinations in Parkinson's disease: a review and phenomenological survey. J Neurol Neurosurg Psychiatry 2001;70:727–733.
3. Sanchez-Ramos JR, Ortoll R, Paulson GW. Visual hallucinations associated with Parkinson disease. Arch Neurol 1996;53:1265–1268.
4. Fenelon G, Mahieux F, Huon R, Ziegler M. Hallucinations in Parkinson's disease: prevalence, phenomenology and risk factors. Brain 2000;123:733–745.
5. Holroyd S, Currie L, Wooten GF. Prospective study of hallucinations and delusions in Parkinson's disease. J Neurol Neurosurg Psychiatry 2001;70:734–738.
6. Goetz CG, Leurgans S, Pappert EJ, Raman R, Stemer AB. Prospective longitudinal assessment of hallucinations in Parkinson's disease. Neurology 2001;57:2078–2082.
7. Okada K, Suyama N, Oguro H, Yamaguchi S, Kobayashi S. Medication-induced hallucination and cerebral blood flow in Parkinson's disease. J Neurol 1999;246:365–368.
8. Friston KJ, Holmes AP, Worsley KJ, Poline JP, Frith CD, Frackowiak RSJ. Statistical parametric maps in functional imaging: a general linear approach. Hum Brain Mapp 1995;2:189–210.
9. Calne DB, Snow BJ, Lee C. Criteria for diagnosing Parkinson's disease. Ann Neurol 1992;32(Suppl.):S125–S127.
10. McKeith IG, Galasko D, Kosaka K, et al. Consensus guidelines for the clinical and pathologic diagnosis of dementia with Lewy bodies (DLB): report of the consortium on DLB international workshop. Neurology 1996;47:1113–1124.
11. Folstein MF, Folstein SE, McHugh PR. "Mini-mental state". A practical method for grading the cognitive state of patients for the clinician. J Psychiatr Res 1975;12:189–198.
12. Hoehn MM, Yahr MD. Parkinsonism: onset, progression and mortality. Neurology 1967;17:427–442.
13. OgawaT. Selection and change of dopamine agonist. In: Yanagisawa N, editor. Parkinson's disease—diagnosis and treatment. Tokyo: Kinbara-shoten; 2000. p 180–188.